# MODIFIED EFFECTIVE CRACK-LENGTH FORMULATIONS IN ELASTIC-PLASTIC FRACTURE MECHANICS

by

**DAGMAR E. HAUF**

Submitted to the Department of
Mechanical Engineering
in Partial Fulfillment of
the Requirements for the Degree of

Bachelor of Science in Mechanical Engineering

at the

MASSACHUSETTS INSTITUTE OF TECHNOLOGY

May, 1992



Signature of Author_____
Department of Mechanical Engineering
May, 1992

Certified by_____
David M. Parks
Professor of Mechanical Engineering
Thesis Supervisor

Accepted by_____
Peter Griffith, Chairman
Departmental Committee on Undergraduate Studies

# Modified Effective Crack-Length Formulations in Elastic-Plastic Fracture Mechanics

by

Dagmar E. Hauf

Submitted to the Department of Mechanical Engineering
on May 8, 1992, in partial fulfillment of the requirements for the
Degree of Bachelor of Science in Mechanical Engineering

## Abstract

Near crack-tip stress fields of linear elastic fracture mechanics (LEFM) are characterized by the first singular term of the Williams eigen-expansion [32]. The magnitudes of these stress fields are conventionally determined by a single parameter, the stress intensity factor $K_I$. A $K_I$ characterization of the near crack-tip fields is limited to the conditions of small-scale yielding (SSY).

Simple but accurate corrections to LEFM are available when moderate yielding occurs. These so-called "effective crack length formulations" correct the actual crack length by a plastic zone correction (corresponding to a fraction of the actual SSY plastic zone) to account for nonlinear effects due to the increasing local crack-tip plasticity. LEFM solutions based on plastically corrected crack lengths can extend LEFM beyond its normal validity limits. At sufficiently high loads, however, the effective crack length formulations become less accurate.

Recently, a marked sensitivity of plastic zone size and orientation to the sign and magnitude of the elastic $T$-stress has been observed. The elastic $T$-stress is the second term in the Williams eigen-expansion of near crack-tip stress fields [32]. Specifically, Larsson and Carlsson [15], using a *Modified Boundary Layer Approach*, found that SSY solutions modified by the elastic $T$-stress can accurately predict the plastic zone shapes and sizes of actual specimens. Based on these observations, the standard effective crack length formulations of LEFM are *modified* to account for the effects of the elastic $T$-stress.

The elastic $T$-stress is shown to consistently extend the range of validity of effective crack length formulations in several specimen geometries. The magnitude of influence of the $T$-stress varies with specimen type and relative crack depth. The greatest improvement to standard effective crack length approximations occurs in specimens of "moderately" negative $T$-stress.

Thesis Advisor: David M. Parks
Title: Professor of Mechanical Engineering

# Acknowledgements

I would like to express my gratitude to Professor David M. Parks for his support and guidance and for giving me the opportunity to work on this project. His enthusiam as a lecturer triggered my interest in the field of fracture mechanics. I would like to thank Hyungyil Lee for sharing his work with me and for his patience in explaining concepts as well as answering questions. I owe special thanks to my mother who, over the past three years, supported me in every way available to her. Most of all, I would like to thank Attilio C. Pisoni, not only for his valuable technical contributions to this work but also for his emotional support and for always being there for me.

# List of Figures

**Fig. 2.14:** Normalized axial force $N$ *vs.* cracked displacement for remote tension of a plane strain $DEN$.

**Fig. 2.15:** Normalized effective crack length *vs.* axial force $N$ for remote tension of a plane strain $DEN$.

**Fig. 2.16:** Normalized $J$ *vs.* axial force $N$ for remote tension of a plane strain $DEN$.

**Fig. 3.1:** Near-crack-tip representation for boundary layer approach [31].

**Fig. 3.2:** Plastic zones in a coordinate system, non-dimensionalized with respect to the characteristic length parameter $(K_I/Y)^2$, of various specimens and BL solution at $K_I = 0.6\,Y\,a^{1/2}$ [15].

**Fig. 3.3:** Plastic zones at a load level $K_I = 0.6\,Y\,a^{1/2}$ for actual geometries and for corrected boundary-value solution [15].

**Fig. 3.4:** The variation of stress triaxiality near a crack tip with respect to $\tau$ in a nonhardening material [7].

**Fig. 3.5:** Normalized crack opening stress profiles at various values of $\tau$. The stresses marked with circles are HRR-singularity fields [31].

**Fig. 3.6:** Angular variation of crack-tip equivalent plastic strain at various $\tau$ [31].

**Fig. 3.7:** Variation of equivalent plastic zone size normalized by the plastic zone size at $\tau = 0$ at various values of $\tau$ ([31]; [16]).

**Fig. 3.8:** Schematic of the plastic zone orientation change at various values of $\tau$. All dimensions of the plastic zone are normalized by the maximum radius of the respective plastic zone [31].

**Fig. 3.9:** Approximate plastic zone shapes according to the von Mises yield criterion applied to the elastic crack-tip stress field [6].

**Fig. 3.10:** Normalized axial force $N$ *vs.* cracked displacement $\delta^c$ of a plane strain

$SEN$ of relative crack depth $a/t = 0.5$ under tension. Good agreement between numerical and continuum solution is found for $\beta = 0.12$. Values of $\beta$ range from $\beta = 0$ to $\beta = 0.24$ in increments of 0.06 [16].

**Fig. 3.11:** $T$-stress calibration function of single edge-cracked specimen under tension [31].

**Fig. 3.12:** $T$-stress calibration function of center-cracked specimen under tension [26].

**Fig. 3.13:** $T$-stress calibration function of double edge-cracked specimen under tension [26].

**Fig. 3.14:** Variation of $\tau$ at 75% of limit load for the $SEN$, $CCP$, and $DEN$ specimens.

**Fig. 3.15:** Normalized axial force $N$ *vs.* cracked displacement for remote tension of a plane strain $SEN$.

**Fig. 3.16:** Normalized effective crack length *vs.* axial force $N$ for remote tension of a plane strain $SEN$.

**Fig. 3.17:** Normalized $J$ *vs.* axial force $N$ for remote tension of a plane strain $SEN$.

**Fig. 3.18:** Normalized axial force $N$ *vs.* cracked displacement for remote tension of a plane strain $CCP$.

**Fig. 3.19:** Normalized effective crack length *vs.* axial force $N$ for remote tension of a plane strain $CCP$.

**Fig. 3.20:** Normalized $J$ *vs.* axial force $N$ for remote tension of a plane strain $CCP$.

**Fig. 3.21:** Normalized axial force $N$ *vs.* cracked displacement for remote tension of a plane strain $DEN$.

**Fig. 3.22:** Normalized effective crack length *vs.* axial force $N$ for remote tension of

a plane strain $DEN$.

**Fig. 3.23:** Normalized $J$ *vs.* axial force $N$ for remote tension of a plane strain $DEN$.

# List of Tables

# Contents

# Chapter 1

# Introduction

## 1.1 Near Crack-Tip Stress Fields

Near crack-tip conditions of both linear elastic fracture mechanics (LEFM) and non-linear elastic fracture mechanics (NLEFM) are characterized by singular stress fields. Conventionally, a single parameter is used to determine the magnitudes of these stress fields, the stress intensity factor $K_I$ in the case of LEFM and the $J$-integral in the case of NLEFM.

One of the basic assumptions behind the application of LEFM to elastic-plastic materials is small-scale yielding (SSY). SSY requires the zone of plastic deformation at the crack-tip to be much smaller than any relevant specimen dimension such as the crack length. Then, the stress state outside the plastic zone, but away from the specimen boundary, can be characterized by the first singular term of the Williams eigen-expansion [32]

$$\sigma_{ij} = \frac{K_I}{\sqrt{2\pi r}} f_{ij}(\theta) \text{ with } K_I = Q\sigma\sqrt{\pi a}, \tag{1.1}$$

where $r$ and $\theta$ are polar coordinates centered at the crack tip as shown in Fig. 1.1, $f_{ij}(\theta)$ are universal angular variations of the respective stress components, $\sigma$ is the nominal stress, and $Q$ is a dimensionless function which depends on the relevant geometrical dimensions. Thus, the stresses vary with the square root of the crack size and tend to infinity at the crack-tip where $r$ is small. Since nominal radial extent of a crack-tip plastic zone under SSY is $r_p^{SSY} \sim \frac{1}{2\pi}(K_I/\sigma_y)^2 \doteq 0.16(K_I/\sigma_y)^2$ [28], the ASTM Standard Test Method for Plane-Strain Fracture Toughness of Metallic Materials [3] specifies that

$$B, a, (W-a) \geq 2.5(\frac{K_I}{\sigma_y})^2 \doteq 16\, r_p^{SSY}, \tag{1.2}$$

where $\sigma_y$ is the tensile yield strength, $a$ is the crack depth, $W$ is the specimen width, $W-a$ is the uncracked ligament, and $B$ is the specimen thickness. By requiring the specimen size to be much larger than the plastic zone size, Eq. (1.2) ensures that the small plastic crack tip is surrounded by a massive elastic domain. Since $K_I$ is proportional to the remote load, the SSY conditions of Eq. (1.2) effectively restrict the magnitude of applied load for a fixed material and geometry.

Linear elastic stress analysis becomes increasingly inaccurate as the inelastic region at the crack tip grows. Simple corrections to LEFM are available when moderate yielding occurs. These approaches correct the actual crack length by a plastic zone correction (corresponding to a fraction of the actual SSY plastic zone) to account

for nonlinear effects due to the increasing local crack-tip plasticity. The resulting effective crack length can be written as

$$a_{eff} = a + r_p^* = a + \Lambda(\frac{K_I}{\sigma_y})^2, \tag{1.3}$$

where $a$ is the actual crack length and $r_p^*$ is the plastic zone size correction. $\Lambda$ is the plastic zone correction factor which depends on the correction model used. LEFM solutions based on plastically corrected crack lengths can extend LEFM beyond its normal validity limits. However, such corrections are only rough approximations of elastic-plastic behavior and typically deviate from continuum solutions at nominal stresses greater than approximately $0.5\sigma_y$. When nonlinear material behavior becomes significant, a crack-tip parameter such as the $J$-integral has to be adopted.

Hutchinson [12] and Rice and Rosengren [22] independently showed that the $J$-integral characterizes crack tip conditions in a nonlinear elastic material. The $J$-integral is defined as the energy release rate in a nonlinear elastic body containing a crack and essentially measures the scale of crack-tip deformation. The line integral expression of $J$ for any contour $\Gamma$ encircling the crack tip in a counterclockwise direction (see Fig. 1.2) is given by

$$J = \int_\Gamma w dy - T_i \frac{\partial u_i}{\partial x} ds, \tag{1.4}$$

where $w$ is the strain energy density, $T_i$ are components of the traction vector acting outward on the contour $\Gamma$, $u_i$ are the displacement vector components, and $ds$ is a

length increment along the contour $\Gamma$. The $J$-integral is independent of the path of integration around the crack provided that there is no crack face traction or body forces and the near crack-tip region undergoes proportional loading. Under SSY conditions the contour $\Gamma$ can be chosen to fall within the region in which the $K_I$-characterized fields hold, thus allowing a relationship between $J$ and $K_I$ to be established as

$$J = \frac{K_I^2}{E'}, \tag{1.5}$$

where $E' = E$ for plane stress and $E' = E/(1-\nu^2)$ for plane strain, $E$ is the Young's modulus, and $\nu$ is Poisson's ratio.

Hutchinson, Rice and Rosengren showed that in order for $J$ to remain path independent, the product of stress and strain must vary as $1/r$ near the crack tip. In a near-crack tip region, where the plastic strains are much larger than the elastic strains, the plastic strain and stress are related by a power law in the form

$$\frac{\varepsilon}{\varepsilon_y} = \alpha(\frac{\sigma}{\sigma_y})^n, \tag{1.6}$$

where $\sigma_y$ is the effective tensile yield stress, $\varepsilon_y = \sigma_y/E$ the associated tensile strain, $n$ is the strain hardening component, and $\alpha$ is a constant. Based on $J_2$-deformation theory of plasticity and small strain asymptotic analysis, the near crack-tip fields within the plastic zone are then given as

$$\sigma_{ij}(r,\theta) \rightarrow \sigma_y\left(\frac{J}{\alpha\varepsilon_y\sigma_y I_n r}\right)^{\frac{1}{n+1}}\tilde{\sigma}_{ij}(\theta,n) \equiv \sigma_{ij}^{HRR}, \tag{1.7}$$

$$\varepsilon_{ij}(r,\theta) \rightarrow \alpha\varepsilon_y\left(\frac{J}{\alpha\varepsilon_y\sigma_y I_n r}\right)^{\frac{n}{n+1}}\tilde{\varepsilon}_{ij}(\theta,n) \equiv \varepsilon_{ij}^{HRR}, \tag{1.8}$$

where $I_n$ is an integration constant that is a function of $n$, and $\tilde{\sigma}_{ij}$ and $\tilde{\varepsilon}_{ij}$ are dimensionless functions that depend on $\theta$ and $n$, and on whether plane strain or plane stress prevail in the vicinity of the crack tip. Eqs. (1.7) and (1.8) are called the HRR singularity. Just as the stress intensity factor $K_I$ determines the magnitude of the asymptotic elastic fields, the $J$-integral defines the strength of the HRR singularity [22].

The HRR stress singularity contains the same apparent anomaly as the LEFM singularity; namely, both predict infinite stresses as $r \rightarrow 0$. The crack-opening stress at $r = 0$ should be bounded, however, since blunting of the crack occurs due to finite strains at the crack tip, thus causing a free surface to be created. Based on a small-scale yielding FE analysis for low hardening and nonhardening materials, McMeeking [18] found that finite strains affect only a region within about 2 to 3 crack tip opening displacements (CTOD's) around the crack tip. McMeeking and Parks [19] performed crack-tip FE analyses based on finite strain $J_2$ incremental plasticity formulation at various load levels from SSY to full plasticity under plane strain conditions. Some of their results are shown in Fig. 1.3. The graph shows normalized stresses as a function of normalized radial distance. Within a distance from the crack tip approximately twice the CTOD, the HRR stress singularity tends to infinity while the crack-opening stress in the finite strain solution decreases as $r \rightarrow 0$. Thus, the HRR stress singular-

ity does not apply within this region. Since the analysis leading to the HRR stress singularity is based on a nonlinear elastic material model, the HRR fields also do not apply where elastic unloading or nonproportional loading exists.

## 1.2 Two-Parameter Characterization of Near Crack-Tip Fields

Whether a near-crack tip field is HRR-dominated depends strongly upon geometry, loading condition, and strain hardening. The geometry dependence is especially strong for low-hardening materials in plane strain. The varied ability of attaining HRR dominance at crack tips of different specimens is attributed to the difference in crack-tip constraint [31]. A widely used constraint parameter is the stress triaxiality, which is defined as the ratio of hydrostatic stress, $\sigma_m = \frac{1}{3}\sigma_{kk}$, to the Mises equivalent stress, $\sigma_e$. Under plane strain conditions, high levels of crack-tip triaxiality are associated with: (a) essentially all states of well-contained yielding; and (b) virtually all load levels in specimens with sufficiently deep cracks under predominately bending load. Conversely, low levels of triaxiality occur in large-scale yielding and fully-plastic flow of single edge-cracked and center-cracked specimens under predominant tension loading, as well as in shallow edge-cracked specimens under bending [20]. A low level of triaxiality generally manifests itself in high macroscopic toughness. McMeeking and Parks [19] proposed that crack-tip stress triaxiality remained sufficiently "high" providing

$$J \leq \frac{\sigma_y l}{\mu_{cr}}, \tag{1.9}$$

where $\mu_{cr}$ is a "critical" lower limit, and $l$ is a characteristic geometric parameter such as the uncracked ligament in a deeply-cracked specimen. Since $J$ is directly related to the applied load magnitude, Eq. (1.9) can be interpreted as a limit for applied load to ensure HRR dominance.

Although the effect of specimen geometry and strain hardening on the attainment of HRR dominance is a relatively well known subject, there is no established criterion to define a crack-tip field as "HRR-dominated". Hancock and co-workers ([5]; [2]; [7]) found that the elastic $T$-stress, which is the second term in the Williams eigen-expansion of near-crack-tip fields [32], may be a useful parameter in quantifying the deviation from HRR singularity fields. Betegón and Hancock [5] showed that the deviation of the crack-opening stress from the SSY solution in various plane strain specimens can be adequately predicted by introducing $T$ as the constraint parameter, even up to large scale yielding. Wang [31] verified the two-parameter characterization of elastic-plastic crack-tip fields ($J$ and $T$) with a 3-D study of stress fields along the crack fronts of plane strain surface-cracked plates ($SCP$s).

## 1.3 Scope of the Work

Chapter 2 examines plastically corrected crack-length formulations. The plastic zone correction of Lee and Parks [16] is used to numerically obtain values of effective crack lengths at specified load levels for $SEN$, $CCP$ and $DEN$ specimens in tension at various crack depths. These plastically corrected crack lengths are used to calculate values of effective stress intensity factors, $K_{I_{eff}}$, of effective elastic $J$-integrals, $J_{eff}$, and of effective cracked displacements, $\delta^c_{eff}$. Results are presented graphically. Plane

strain elastic-plastic FE analyses of the specimens are conducted to compare the plastically corrected LEFM results with results of NLEFM. The extent to which solutions based on effective crack lengths can extend the validity of LEFM formulations is investigated.

Chapter 3 introduces the concept of the elastic $T$-stress and discusses its use as a second parameter to characterize the near-crack fields. Based on the two-parameter characterization of the HRR-dominated crack-tip fields, the effectiveness of the elastic $T$-stress in extending the validity of the plastically corrected LEFM formulations is investigated. As it has been found that the plastic zone size is more sensitive to the change of $T$-stress than any other crack-tip feature, the plastic zone correction factor, $\Lambda$, determining the magnitude, and therefore the size, of the plastic zone correction is formulated as a function of the elastic $T$-stress. Results are compared with the effective crack-length results of Chapter 2 and the corresponding elastic-plastic FE solutions.

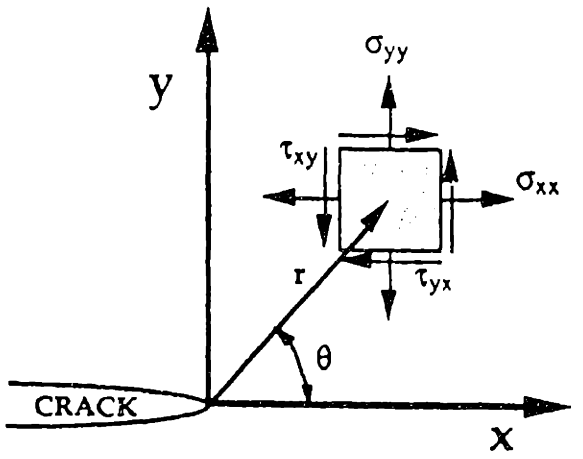


Figure 1.1: Geometry of near crack-tip region [1].

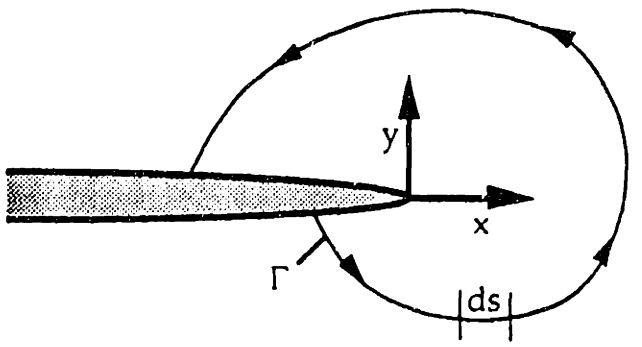


Figure 1.2: Contour definition of the $J$-integral [1].

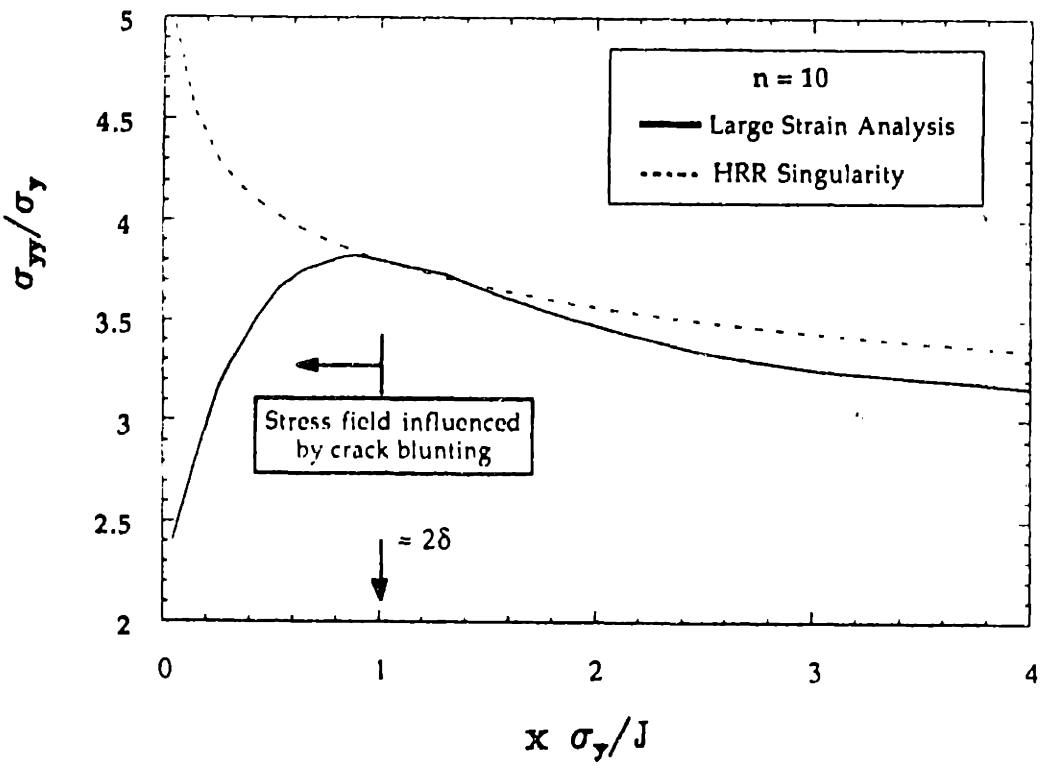


Figure 1.3: Finite strain crack-tip FE results of McMeeking and Parks [1].

# Chapter 2

# Effective Crack-Length Formulations

## 2.1 Crack-Tip Plasticity

According to the elastic stress field solutions discussed in the previous chapter, LEFM predicts infinite stresses at the tip of an elastic crack. However, since materials exhibit a yield stress above which they deform plastically, there must be a region around the crack tip (as $r \rightarrow 0$) where plastic deformation occurs and a $r^{-1/2}$ stress singularity cannot exist. This region is known as the crack-tip plastic zone.

Irwin [14] argued that the occurence of crack-tip plasticity makes the crack behave as if it were longer than its physical size. As a result, the displacements work-conjugate to applied loading are larger and the secant stiffness is lower than in the elastic case. In other words, the specimen behaves as if it contained an elastic crack of somewhat larger size. To account for this difference in macroscopic behavior, Irwin used an effective crack length which he defined as the sum of the actual crack size and a

plastic zone correction (corresponding to half the size of the plastic zone).

LEFM solutions based on plastically corrected crack length formulations can extend LEFM beyond its normal validity limits. Numerous methods (yielding different results) for obtaining the plasticity correction term have been developed. The Irwin plastic-zone correction model, the Dugdale model, and the Edmunds and Willis model are presented here.

## 2.2 The Irwin Plastic-Zone Correction

Using linear elastic analysis, the crack opening stress in the crack plane ($\theta = 0$) can be expressed by the first term of the Williams eigen-expansion [32] as

$$\sigma_{yy} = \frac{K_I}{\sqrt{2\pi r}}, \tag{2.1}$$

where $K_I$ is the stress intensity factor, and $r$ is the radial distance from the crack tip. Fig. 2.1 shows $\sigma_{yy}$ as a function of $r$. Up to a distance $r_y$ from the crack tip (equal to the size of the plastic zone) the stress is higher than the yield strength $\sigma_y$. A rough estimate of $r_y$ can be obtained by replacing $\sigma_{yy}$ in Eq. (2.1) by the yield strength of the material. For plane stress, $r_y$ is thus given as

$$r_y = \frac{1}{2\pi}(\frac{K_I}{\sigma_y})^2. \tag{2.2}$$

It is easy to see that the actual plastic zone size must be larger than the plastic

zone size predicted by Eq. (2.2) since the load represented by the shaded region must be redistributed to the region immediately ahead of the plastic zone to satisfy equilibrium. This redistribution results in higher stresses in the region immediately ahead of the first-order plastic zone. Based on these observations, a second-order estimate of the plastic zone size can be obtained from a simple force balance as

$$r_p = \frac{1}{\pi}(\frac{K_I}{\sigma_y})^2, \tag{2.3}$$

which is twice as large as the first-order estimate in Eq. (2.1).

To account for the occurence of plasticity at the crack tip Irwin [14] proposed the use of an effective crack length (extending to the center of the plastic zone; see Fig. 2.2) which he defined as the sum of the actual crack size and a plastic zone correction. Thus,

$$a_{eff} = a + r_p^*. \tag{2.4}$$

The correction term $r_p^*$ is known as the Irwin plastic-zone correction. Its magnitude equals half the size of the plastic zone. For plane stress $r_p^*$ equals $r_y$ in Eq. (2.2). In plane strain, yielding is suppressed by triaxiality, and the correction term is smaller by a factor of three, thus

$$r_p^* = \frac{1}{6\pi}(\frac{K_I}{\sigma_y})^2. \tag{2.5}$$

## 2.3 The Dugdale Approach

A different approach was followed by Dugdale [8] and Barenblatt [4]. They also consider an effective crack which is longer than the physical crack as in Fig. 2.3. At the crack edges a plastic zone of length $\rho$ carries the yield stress $\sigma_y$, tending to close the crack. The length $\rho$ is chosen so that the stress singularity at the tip of the effective crack disappears [6]. That is, the stress intensity factor due to the remote tension, $K_{I\sigma}$, and the stress intensity factor due to the closure stress, $K_{I\rho}$, cancel each other, so

$$K_{I\sigma} = -K_{I\rho}. \tag{2.6}$$

The stress intensity due to the closure stress $K_{I\rho}$ can be estimated by considering a closure force $dP = -\sigma_y\, dx$ applied to the crack at a distance $x$ from the center line of the crack (see Fig. 2.4). The infinitesimal stress intensity factors for the two crack tips generated by the wedge loads are then given by

$$dK_{I(+a)} = \frac{dP}{\sqrt{\pi a}}\sqrt{\frac{a+x}{a-x}} \tag{2.7}$$

$$dK_{I(-a)} = \frac{dP}{\sqrt{\pi a}}\sqrt{\frac{a-x}{a+x}}. \tag{2.8}$$

$K_{I\rho}$ is obtained by replacing "$a$" with "$a+\rho$" in Eqs. (2.7) and (2.8) and by adding

and integrating the contributions from both crack tips. Thus,

$$K_{I\rho} = -2\sigma_y\sqrt{\frac{a+\rho}{\pi}}\cos^{-1}(\frac{a}{a+\rho}). \tag{2.9}$$

According to Eq. (2.6) this stress intensity has to be equal to $K_{I\sigma}$, where, for the Griffith crack configuration, $K_{I\sigma} = \sigma\sqrt{\pi(a+\rho)}$. Therefore,

$$\frac{a}{a+\rho} = \cos\frac{\pi\sigma}{2\sigma_y}. \tag{2.10}$$

Neglecting higher order terms in the Taylor series expansion of the cosine function, the plastic zone size $\rho$ is obtained as

$$\rho = r_p = \frac{\pi}{8}(\frac{K_I}{\sigma_y})^2, \tag{2.11}$$

where $K_I = \sigma\sqrt{\pi a}$.

Comparison of this result with the result from the Dugdale model, Eq. (2.11), shows that the two approaches predict similar plastic zone sizes.

## 2.4 The Edmunds and Willis Approach

Edmunds and Willis [9] used the method of matched expansions [29] to obtain plastic zone corrections. This procedure generates complementary asymptotic expansions in a loading parameter $\varepsilon$, which are valid close and far from the crack field. The leading

terms of these expansions constitute the LEFM small-scale yielding approximation, while succeeding terms produce corrections that become significant at higher load levels. The method allows the linear elastic far-field to be considered separately from the elastic-plastic near-tip field, except for coupling through a set of parameters which are determined in the matching. The effects of plasticity appear in these parameters only through a set of constants $C_i$. These constants are material constants, which depend upon the constitutive relation for the material, but not upon specimen geometry and loading.

Using this method, the plasticity correction term $r_p^*$ of the effective crack length $a_{eff} = a + r_p^*$ can be expressed as

$$r_p^* = \frac{C_1}{4\pi}(\frac{K_I}{\sigma_y})^2. \tag{2.12}$$

For the Dugdale model $C_1$ can be shown to equal $\frac{\pi^2}{6}$. Substituting this value into Eq. (2.12), the plastic zone-size correction for the Dugdale model is obtained as

$$r_p^* = \frac{\pi}{24}(\frac{K_I}{\sigma_y})^2, \tag{2.13}$$

which is one third of the estimate given in Eq. (2.11).

For an elastic-perfectly plastic material satisfying the Mises yield criterion the value of the constant $C_1$ is 0.24 which, upon substitution in Eq. (2.12), gives the plastic zone-size correction as

$$r_p^* \approx 0.019 \left(\frac{K_I}{\sigma_y}\right)^2. \tag{2.14}$$

This is approximately one third the conventional value in Eq. (2.5).

## 2.5 Formulation

To investigate to which extent a plastically corrected crack length can extend the validity of LEFM formulations, graphs of $J$-integral *vs.* tensile load $N$ and load $N$ *vs.* cracked displacement $\delta^c$ were generated. Following the work of Lee and Parks [16], which will be discussed in Chapter 3, a plastic zone correction factor $\Lambda$ of 0.018 was used. This factor is almost identical to the Edmund and Willis correction factor for an elastic-perfectly plastic material satisfying the Mises yield criterion and close to the correction factor Sham determined (0.025) [24] using the modified variational principle for SSY of Hilton and Hutchinson [11]. The effective crack length can thus be written as

$$a_{eff} = a + 0.018 \left(\frac{K_I(a_{eff}, t)}{\sigma_y}\right)^2. \tag{2.15}$$

$K_I$ itself depends on the current loads and the effective crack length implicitly. The stress intensity factor appearing in Eq. (2.15) due to the load $N$ is thus given by

$$K_I(a_{eff}, t) = \hat{k}(a_{eff}, t)\, \sigma_{nominal}, \tag{2.16}$$

where $\sigma_{nominal}$ is the nominal stress, which in terms of the tensile load $N$ can be expressed as $N/t$ for all three specimens if in the case of the $CCP$ and $DEN$ specimens symmetry conditions are imposed; that is, only half of the specimen is considered ($\sigma_{nominal_{DEN}} = \sigma_{nominal_{CCP}} = 2N/2t$). The function $\hat{k}(a,t)$ contains the $K_I$-calibrations of the specimen under consideration. These calibration functions can be obtained from handbooks; e.g., Tada, et al. [27].

From Eqs. (2.16) and (1.5) it is clear that the elastic expression of the $J$-integral must be a function of the effective crack length. Thus,

$$J(a_{eff},t) = \frac{K_I^2(a_{eff},t)}{E'}. \tag{2.17}$$

The remote displacement, $\delta$, of a specimen due to a load $N$ can be decomposed into

$$\delta = \delta|^{no\,crack} + \delta|^{crack}, \tag{2.18}$$

where $\delta|^{no\,crack}$ is the displacement of the uncracked specimen and $\delta|^{crack}$ is the displacement due to the additional compliance introduced to the specimen by the presence of the crack. In the linear elastic range, the cracked displacement, $\delta^c$, for a given load, $N$, is given by

$$\delta^c(a,t) = C(a,t)\,N, \tag{2.19}$$

where $C(a,t)$ is the elastic compliance. $C(a,t)$ is determined from the Mode I stress

intensity factor calibrations of the specimen using energy/compliance relation as [23]

$$C(a,t) = \frac{2}{E'}\frac{1}{t^2}\int_0^a \hat{k}^2(\bar{a},t)d\bar{a}. \tag{2.20}$$

Introduction of an effective crack length instead of the actual crack length makes the compliance $C(a,t)$ a function of $a_{eff}$, that is

$$C(a_{eff},t) = \frac{2}{E'}\frac{1}{t^2}\int_0^{a_{eff}} \hat{k}^2(\bar{a},t)d\bar{a}, \tag{2.21}$$

which in turn influences the load/displacement relationship of Eq. (2.19). Thus,

$$\delta^c(a_{eff},t) = C(a_{eff},t)\,N. \tag{2.22}$$

It is to be noticed that, since in the case of the $DEN$ and $CCP$ specimens only half of the specimen (and therefore only one crack-tip extension) was considered, the actual compliance $C(a_{eff},t)$ is half of that obtained with Eq. (2.21). In other words, the applied loads for which the corresponding displacements are calculated have to be multiplied by a factor of two to obtain the correct results. In our computational procedure, Eqs. (2.15, 2.16) were solved with the Newton-Raphson method [21]. The integral in Eq. (2.21) was evaluated with a 10-point Gaussian integration [21]. A listing of the program for the $SEN$ specimen is shown in the Appendix.

## 2.6 Elastic-Plastic FE Analysis

The mesh used in the FE analysis is shown in Fig. 2.6. It is the same mesh Lee and Parks [16] used in a recent work to enhance the elastic-plastic line-spring finite element with an effective crack length. They studied the effect of an effective crack length based on a strain hardening material model throughout the plastic regime. The crack-tip is modeled by a rectangular domain shown in Fig. 2.7. There are eight fans of elements, each fan containing four elements radially. The innermost element (at the crack tip) is degenerated so one side collapsed into a single point at the crack tip. Lee and Parks used this element since one of the crack-tip governing parameters they investigated was the crack-tip opening displacement. Plane strain, 8-node, reduced integration elements (ABAQUS element type CPE8R [10]) were used. FE analyses were performed on $SEN$, $DEN$, and $CCP$ specimen in tension at three different crack depths ($a/t = 0.5, 0.35,$ and $0.2$). To obtain the displacement only due to the presence of the crack as a function of imposed load, the displacement of the uncracked specimen (also obtained by FEA) was subtracted from the total displacement, that is, $\delta^c = \delta - \delta^{nc}$. Taking advantage of symmetry, only half of the $SEN$ specimen was modeled with symmetry boundary condition imposed on the plane $y = 0$. For both the $DEN$ and the $CCP$ specimen, symmetry allowed modeling of only one quarter of the specimen (see Fig. 2.5). For the $DEN$ specimen, symmetry boundary conditions were imposed in the planes $x = (t - a)$ and $y = 0$, while for the $CCP$ specimen symmetry boundary conditions were imposed in the planes $x = -(t - a)$ and $y = 0$.

The material considered is ASTM A710 Grade A steel. The material was modeled as isotropic elastic-plastic, with isotropic hardening. The yield strength was given

as a function of the equivalent plastic strain, with an initial value of $\sigma_y = 68.2\,ksi$ ($469.9\,MPa$) and a saturation value of $98.3\,ksi$ ($677.3\,MPa$). A value of $t = 1\,in$ was used for all three specimens. Unit depth into the plane was assumed.

## 2.7 Results and Discussion

The normalized load/deflection curves of the three specimens are shown in Figs. 2.8, 2.11, and 2.14. Curves of normalized $J$ *vs.* normalized $N$ are presented in Figs. 2.10, 2.13, and 2.16. Figs. 2.9, 2.12, and 2.15 show the evolution of the effective crack length of the three specimens with increasing load. For the purpose of comparison, the obtained results were analyzed by determining at what fraction of limit load (obtained from elastic-perfectly plastic FE analysis with $\sigma_y = 68.2\,ksi$, see Table 2.1 for values) deviation from the continuum solution would take place. Deviation was considered to occur when the displacements of the LEFM or the plastically corrected solution at a given load level varied from the displacement of the continuum solution at the same load level by approximately 1%.

Table 2.1: Limit loads (in *lb/in*) obtained by elastic-plastic FE analysis.

| | SEN specimen | CCP specimen | DEN specimen |
|---|---|---|---|
| $a/t = 0.2$ | 62,131 | 125,974 | 140,028 |
| $a/t = 0.35$ | 44,623 | 102,430 | 125,055 |
| $a/t = 0.5$ | 39,125 | 79,050 | 107,473 |

A general improvement of the plastically corrected solutions compared to the LEFM solutions can be noted. This improvement is observed as a shift of the curves of plastically corrected solutions towards the continuum solution.

More specifically, for the $SEN$ specimen of relative crack depth 0.5, deviation of the plastically corrected solution from the continuum solution occurs at a load level corresponding to approximately 37% of limit load compared to a first deviation of the corresponding LEFM solution at approximately 23% of limit load. Thus, the plastically corrected solution increases the load range of accurate solution by a fraction of limit load of approximately 14%. Similarly, the cracks of length 0.35 and 0.2 show an increase in load range of accurate solution of approximately 11% and 12%, respectively. For the $CCP$ specimen, use of an effective crack length extends the load range of accurate solution by approximately 6% of limit load for the 0.2 crack and by approximately 9% for the cracks of length 0.35 and 0.5. For the $DEN$ specimen, load ranges of accurate solution are increased by approximately 15% of limit load for the 0.2 crack and by approximately 17% for the cracks of length 0.35 and 0.5. No clear trends of increasing (or decreasing) load range of accurate solution with increasing relative crack depth can be observed in any of the specimens.

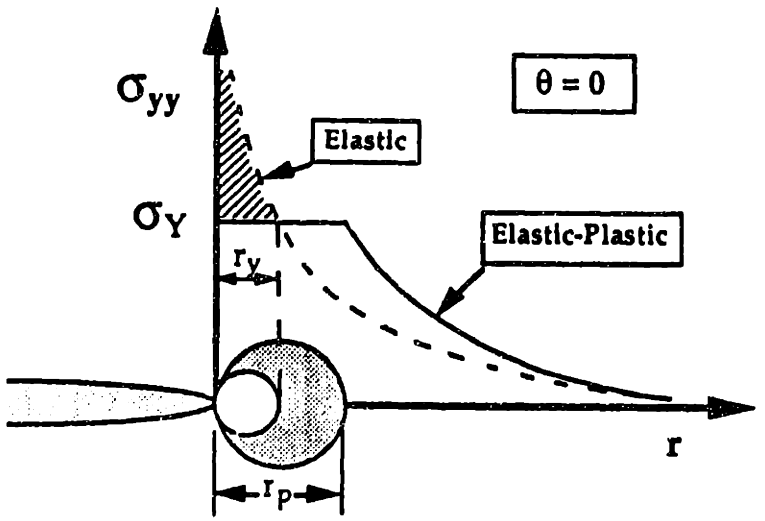


Figure 2.1: First and second-order estimates of the plastic zone size [1].

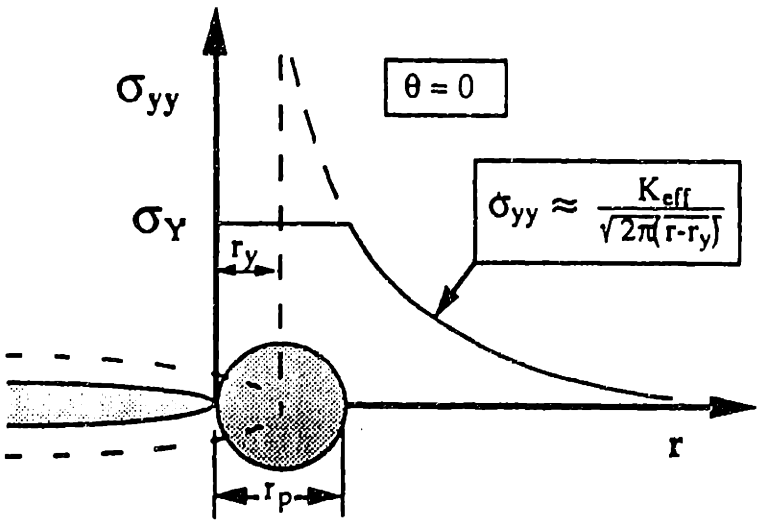


Figure 2.2: Irwin's plastic zone correction [1].

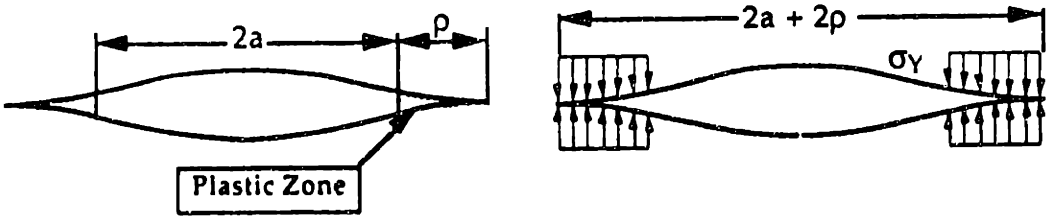


Figure 2.3: The Dugdale approach [1].

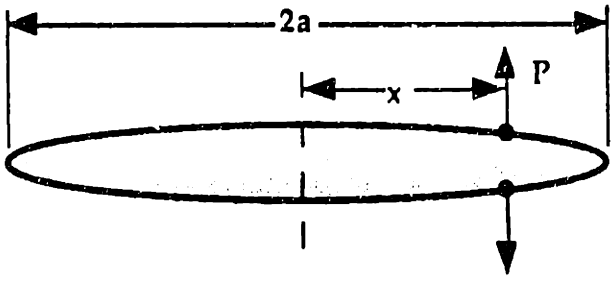


Figure 2.4: Wedge force applied at a distance $x$ from the center line [1].

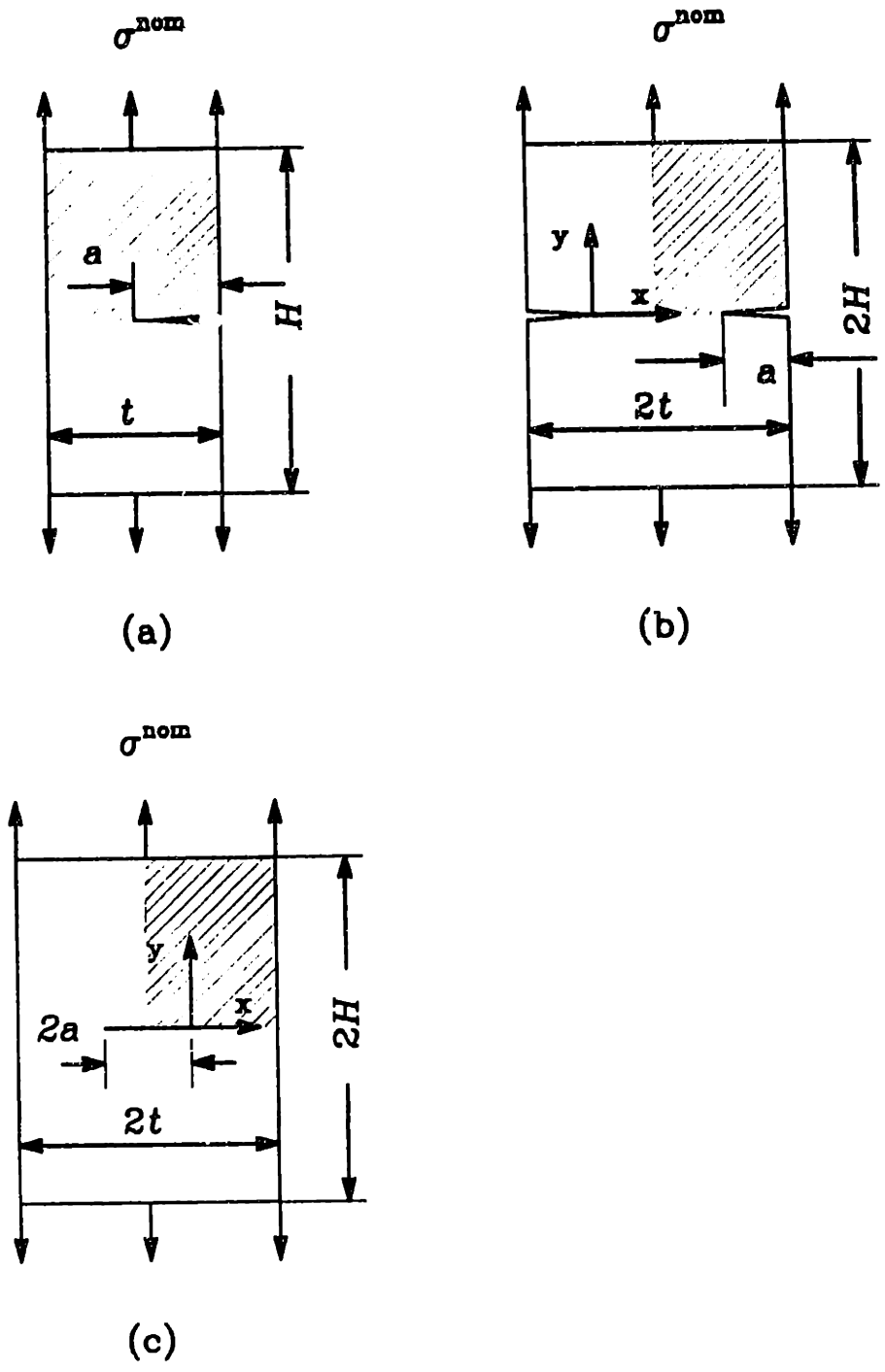


Figure 2.5: Specimen geometries (for symmetry reasons only shaded parts are considered): (a) single edge-cracked specimen; (b) double edge-cracked specimen; (c) center-cracked specimen.

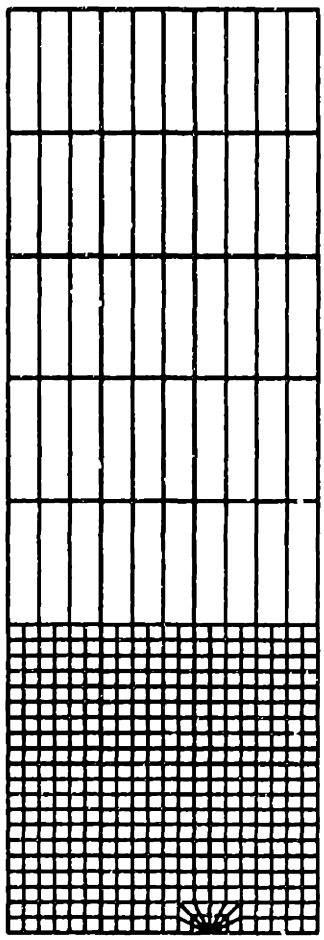

Figure 2.6: FE mesh used in analysis.

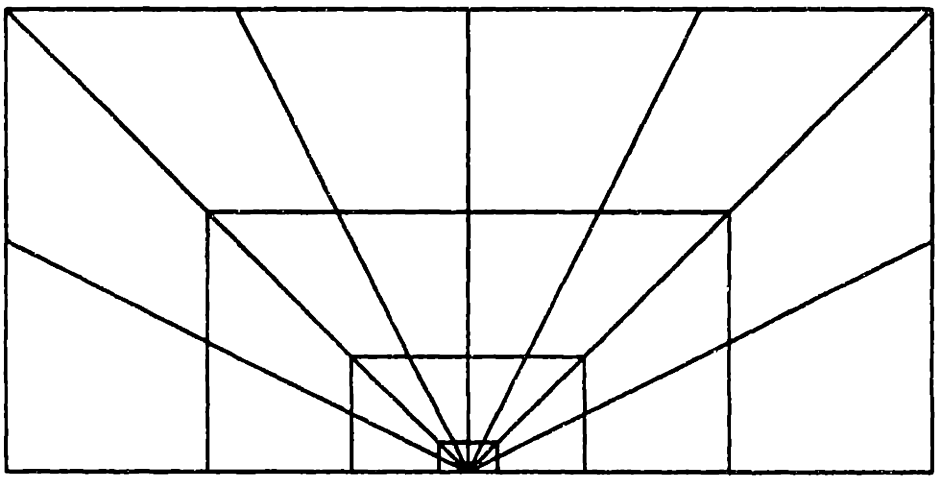

Figure 2.7: FE representation of crack-tip region.

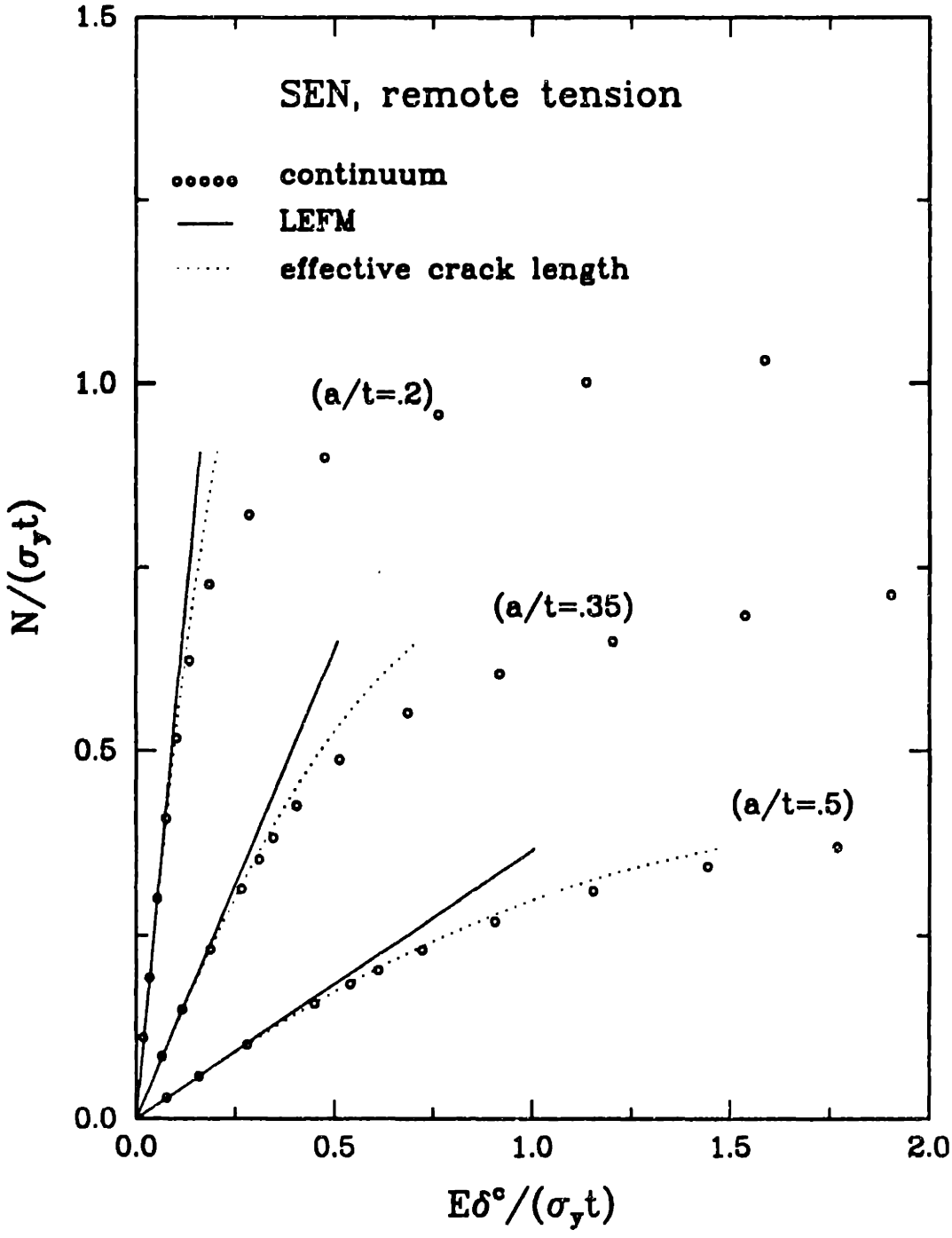


Figure 2.8: Normalized axial force $N$ *vs.* cracked displacement for remote tension of a plane strain $SEN$.

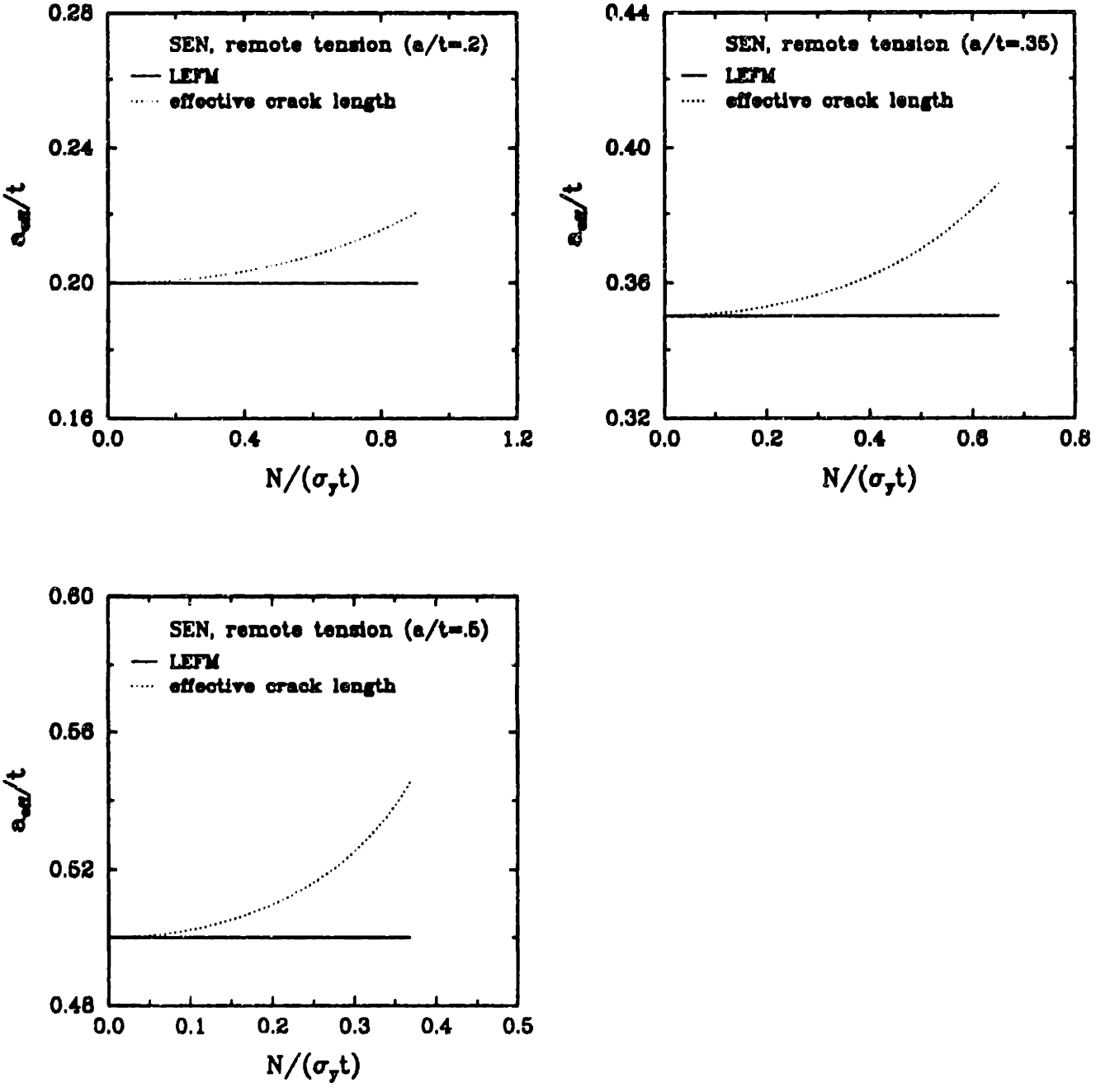


Figure 2.9: Normalized effective crack length *vs.* axial force $N$ for remote tension of a plane strain $SEN$.

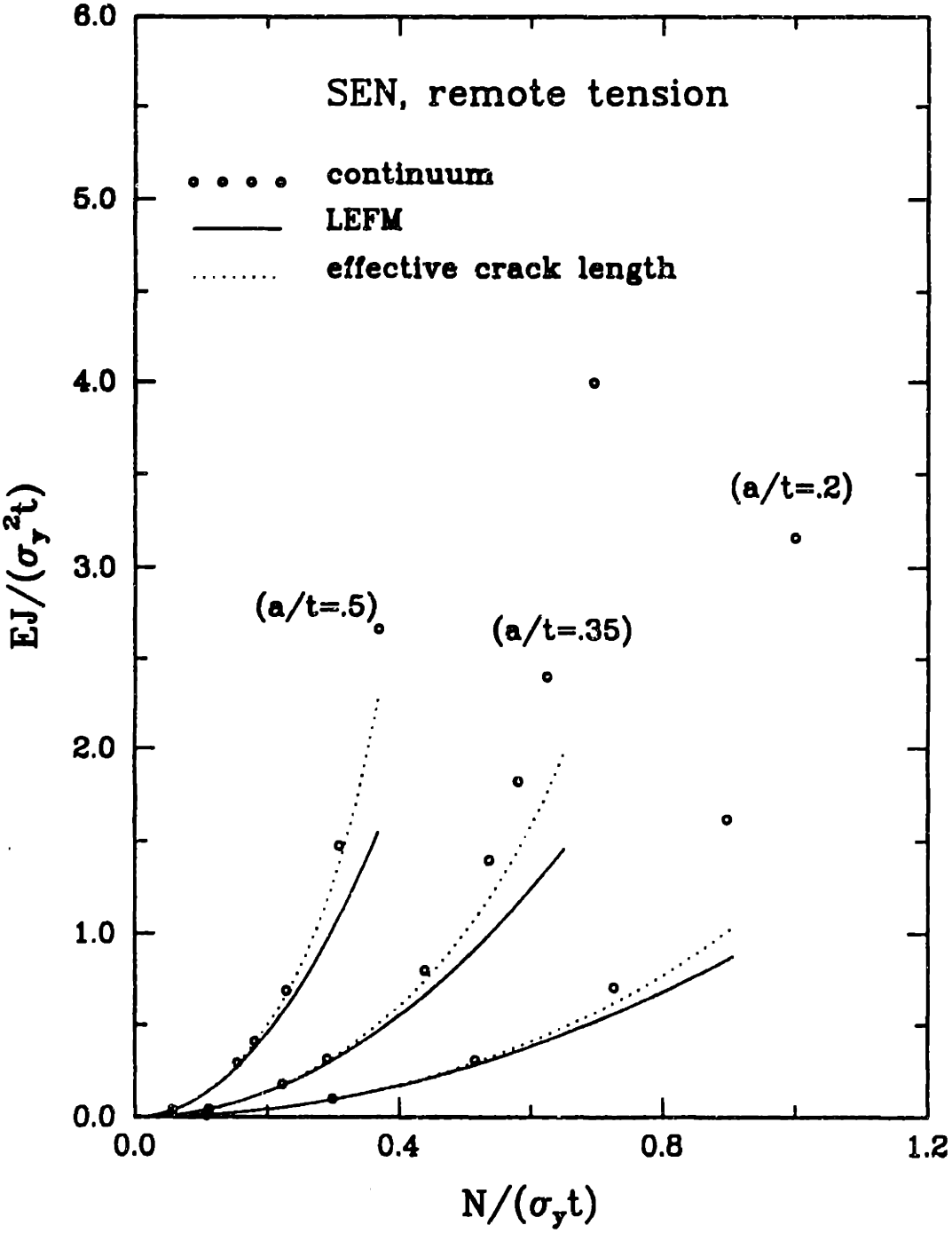


Figure 2.10: Normalized $J$ *vs.* axial force $N$ for remote tension of a plane strain *SEN*.

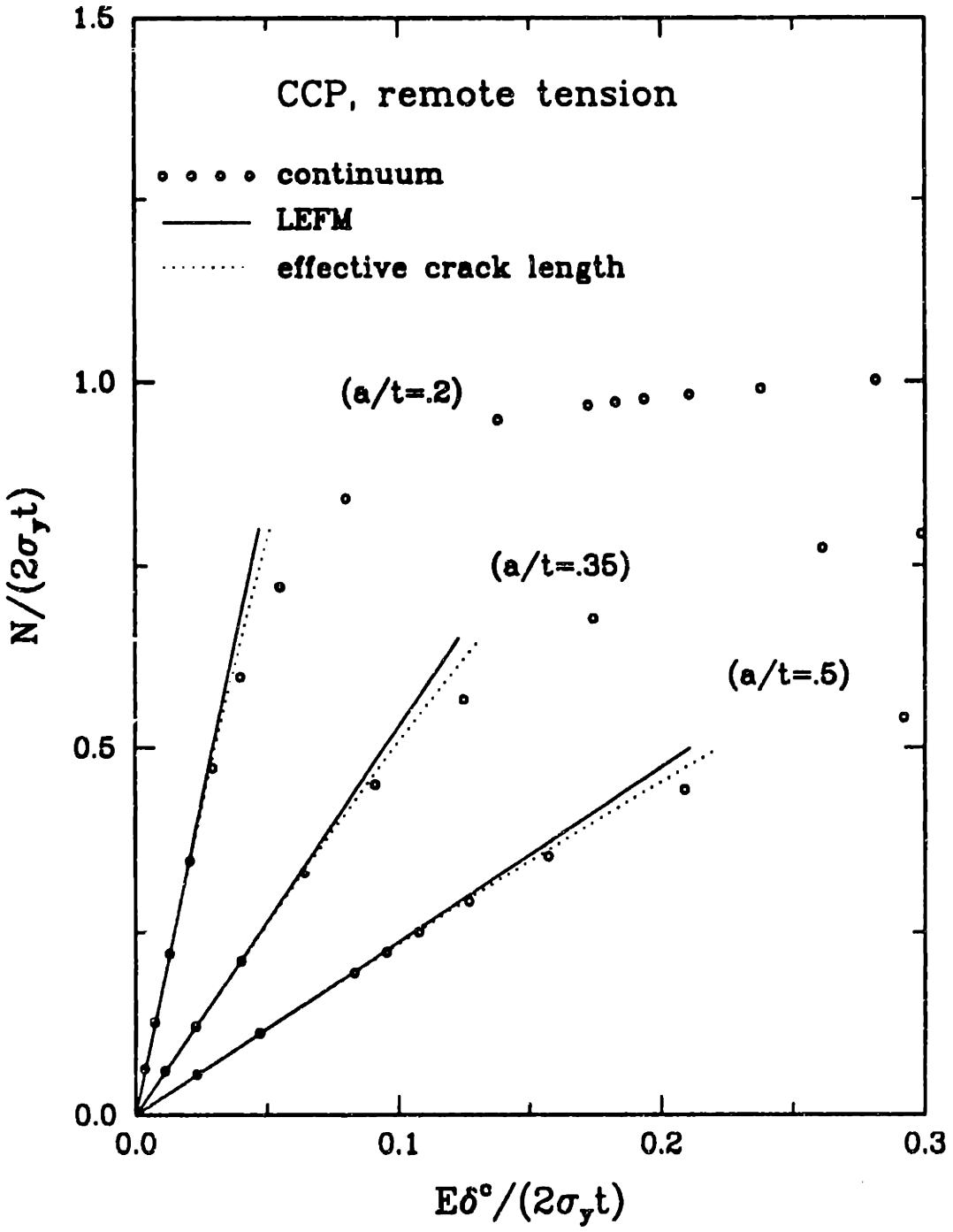


Figure 2.11: Normalized axial force $N$ *vs.* cracked displacement for remote tension of a plane strain $CCP$.

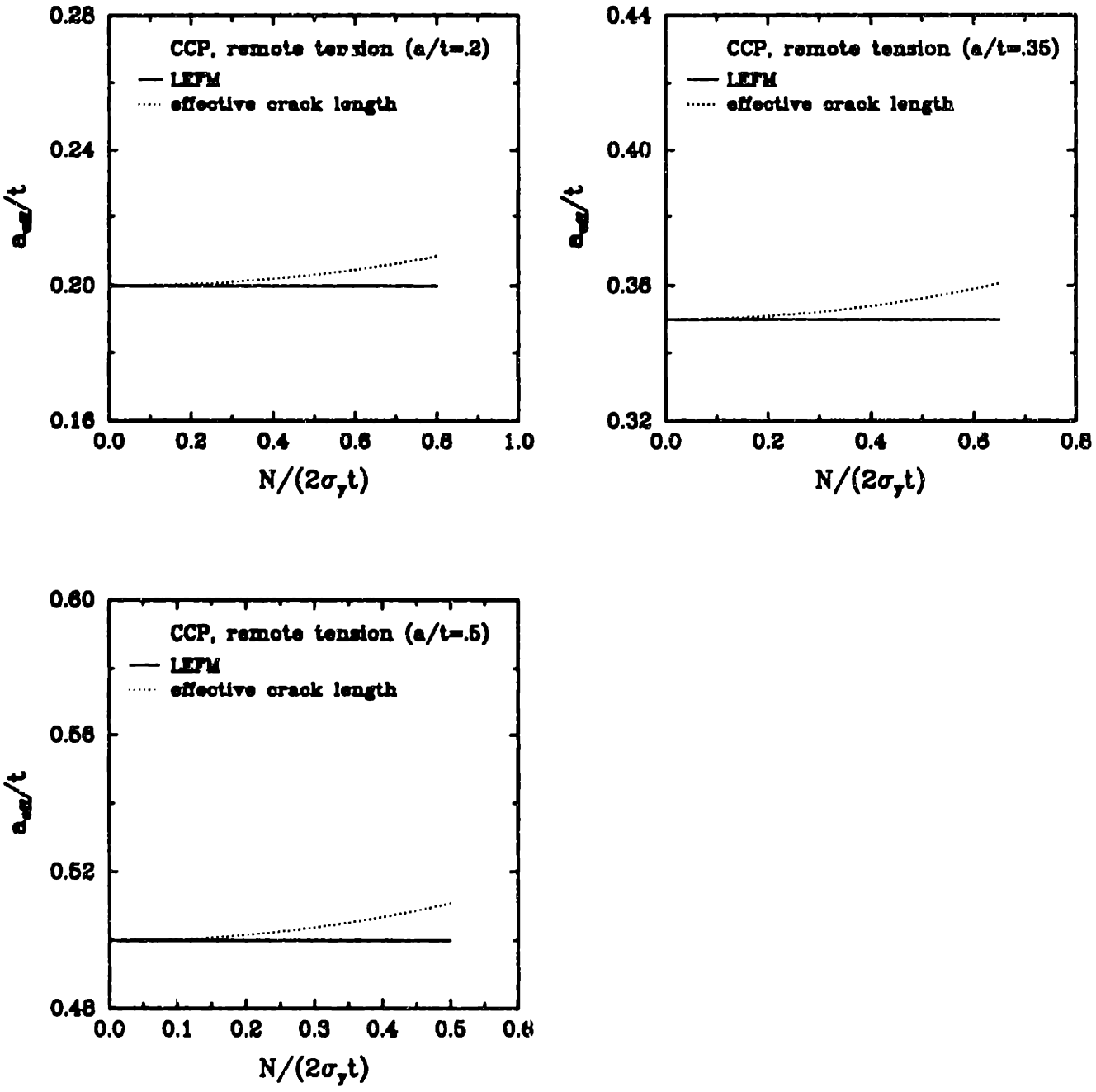


Figure 2.12: Normalized effective crack length *vs.* axial force $N$ for remote tension of a plane strain $CCP$.

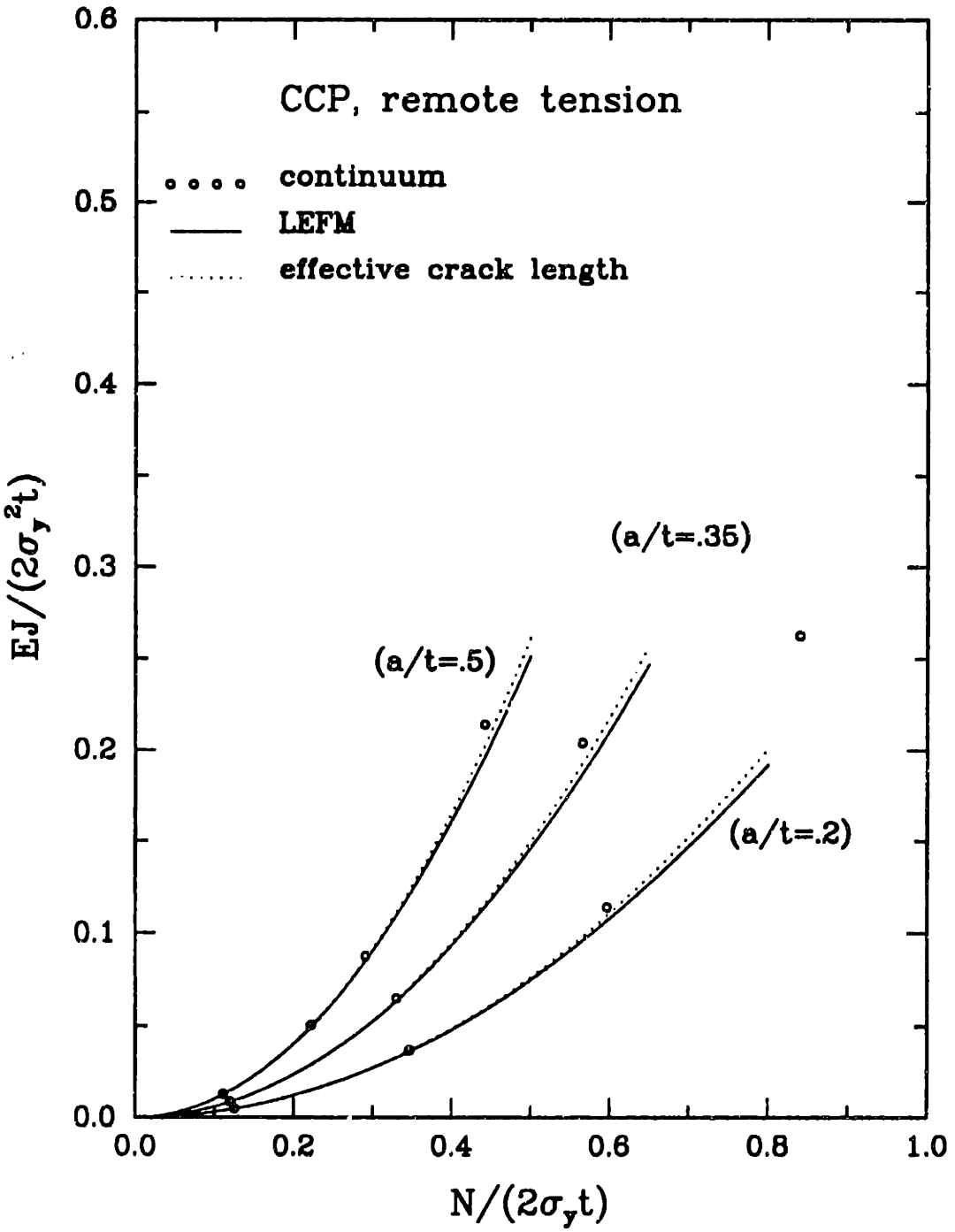


Figure 2.13: Normalized $J$ *vs.* axial force $N$ for remote tension of a plane strain *CCP*.

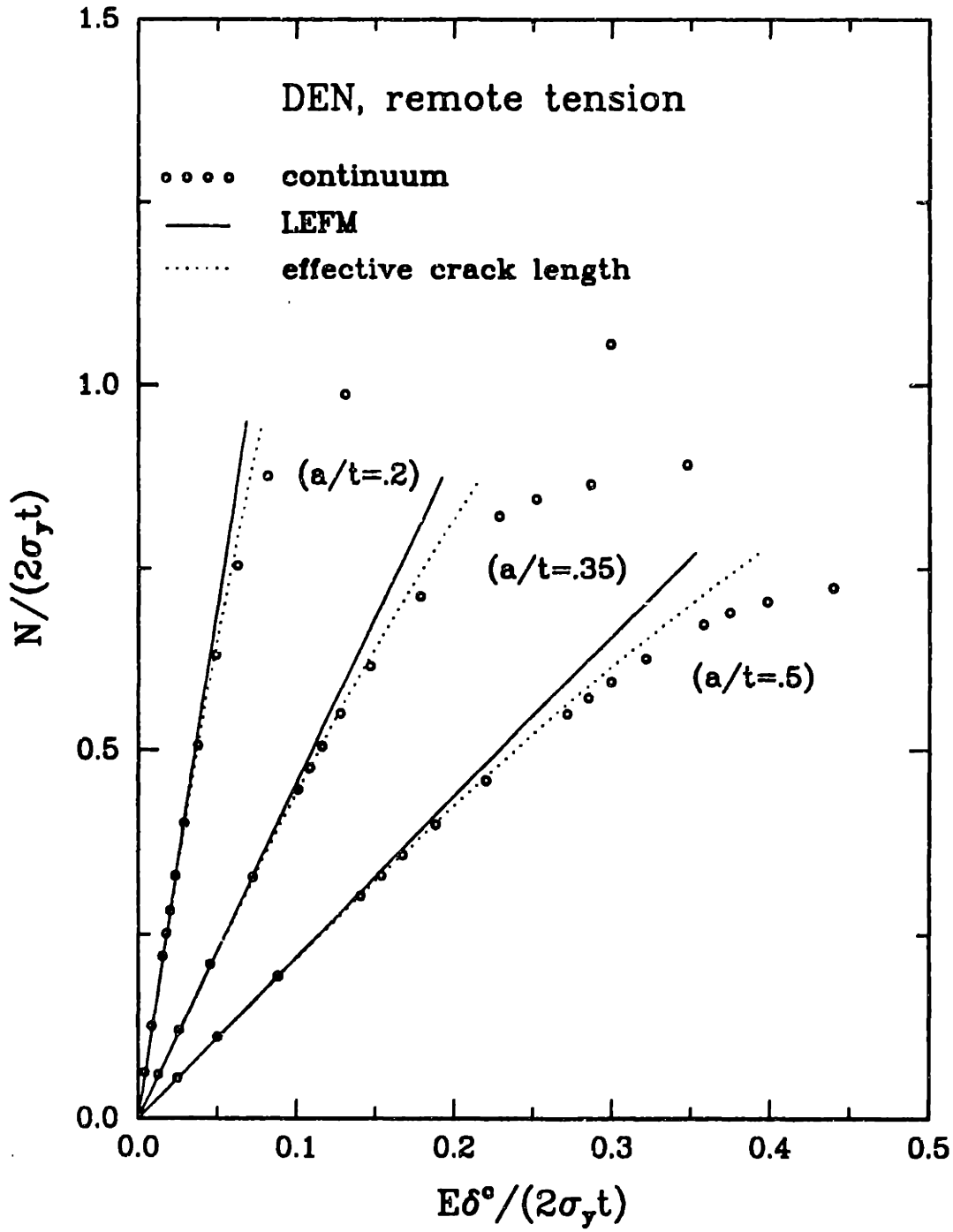


Figure 2.14: Normalized axial force $N$ *vs.* cracked displacement for remote tension of a plane strain *DEN*.

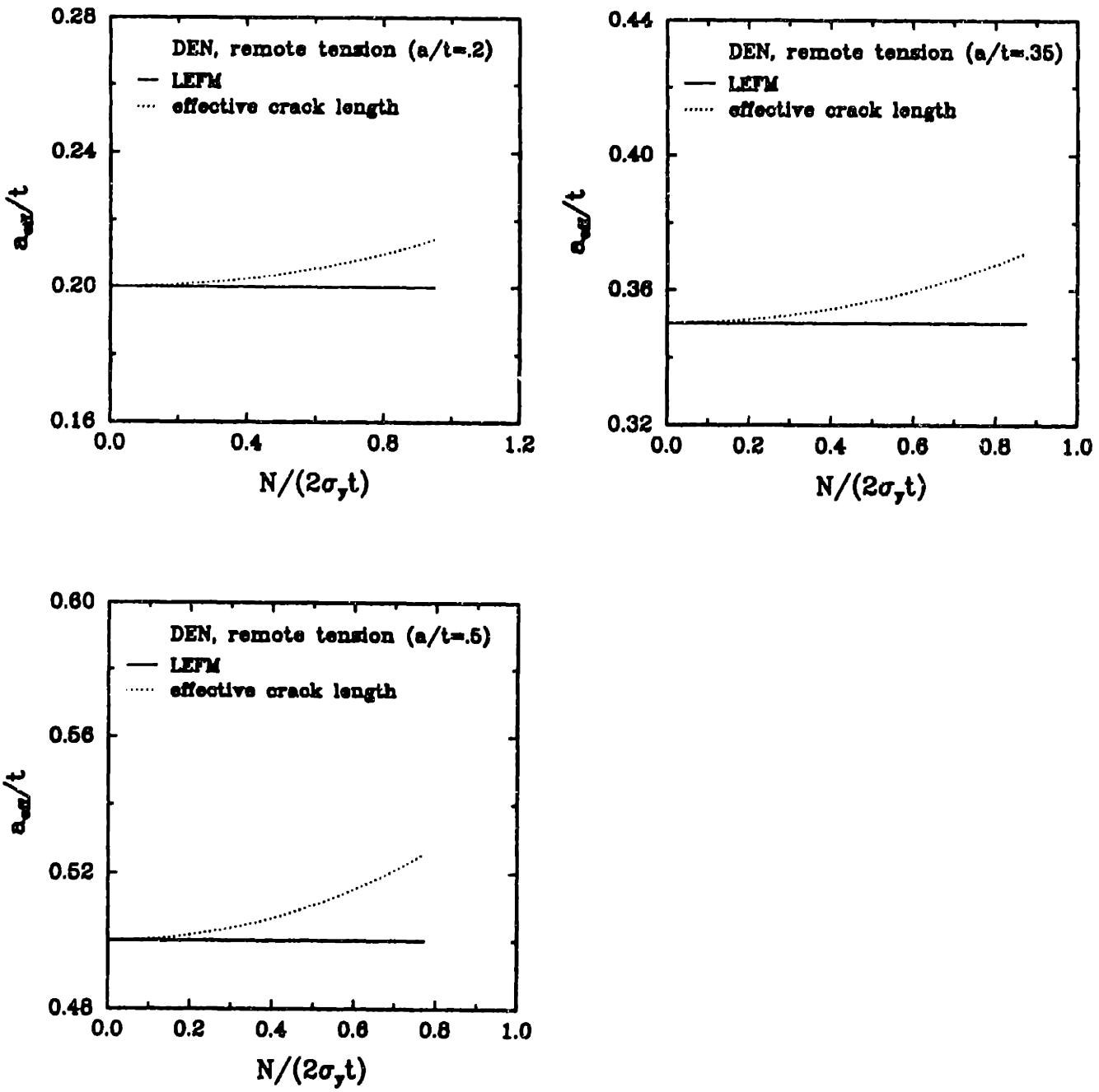


Figure 2.15: Normalized effective crack length *vs.* axial force $N$ for remote tension of a plane strain *DEN*.

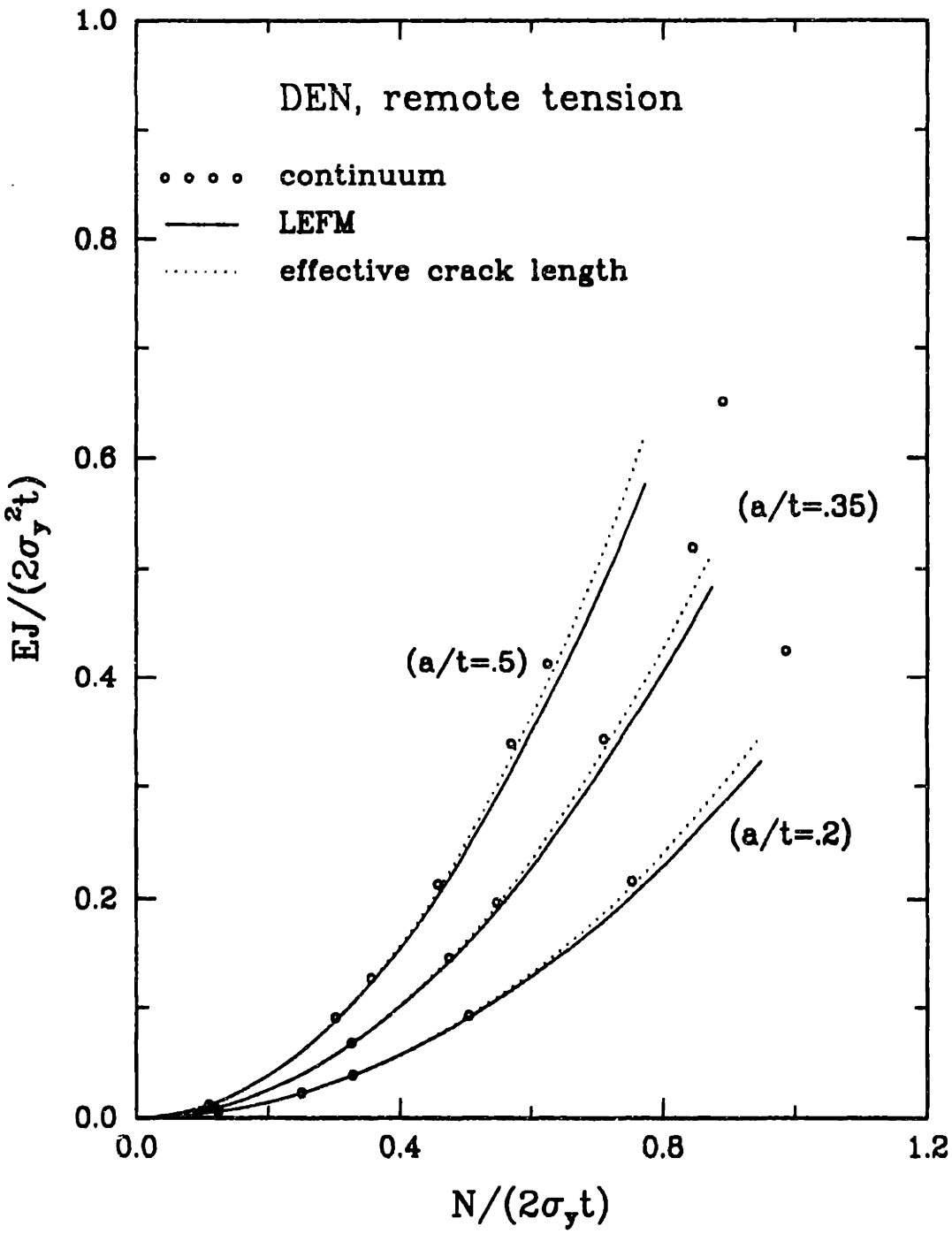


Figure 2.16: Normalized $J$ *vs.* axial force $N$ for remote tension of a plane strain *DEN*.

# Chapter 3

# $T$-Stress and Modified Effective Crack-Length Formulations

## 3.1 The Elastic $T$-Stress

Under the conditions of SSY, that is, if the state at the crack tip in an elastic-plastic material at low load levels is uniquely determined by $K_I$, the crack problem can be solved by using a "boundary layer" (BL) approach [15]. This BL solution assumes that the stresses on the boundary of a circle of radius $R$ centered at the crack-tip (see Fig. 3.1) are those defined by the singular elastic stress fields of Eq. (1.1). The value of $K_I$ is hereby taken to be the same as that of the actual specimen and loading. The extent to which the near-crack-tip fields of the BL solution and those of an actual specimen agree with each other is an indication of the validity of the $K_I$-based one-parameter characterization of crack-tip fields under SSY conditions.

Larsson and Carlsson [15] performed plane strain elastic-plastic FE analyses on four commonly employed test specimens with a variety of crack-tip constraints under SSY

conditions and compared their results with corresponding plane strain BL solutions. The normalized crack-tip plastic zones of the four specimens and the BL solution at a load level $K_I = 0.6\,\sigma_y\sqrt{a}$, where $a$ is the crack length, are shown in Fig. 3.2. Clearly, the normalized sizes and shapes of the plastic zones are different from the BL solution. Only if the plastic state were determined by $K_I$ alone would the plastic zones for the different cases coincide [15]. Larsson and Carlsson argued that this difference is due to the representation of the near-crack-tip stress field by only the leading term of the Williams expansion. The second term is a constant tension or compression $T$-stress parallel to the crack, and the succeeding terms approach zero as $r \to 0$. The stress field in the crack-tip region can thus more acccurately be described by

$$\sigma_{ij} = \frac{K_I}{\sqrt{2\pi r}} f_{ij}(\theta) + T\delta_{1i}\delta_{1j}, \tag{3.1}$$

where $T$ represents the $T$-stress, and $\delta_{1i}$, $\delta_{1j}$ are Kronecker deltas. The $T$-stress is not singular as $r \to 0$, but it can alter the crack-tip stress state, thus *modifying* the crack-tip plastic zone. Like $K_I$, the $T$-stress in Eq. (3.1) is a function of geometry, loading conditions, and load magnitude ([15]; [17]; etc.). For instance, specimens under predominately tension load often have large negative $T$-stress, and deep-cracked specimens under bending often have a less negative $T$-stress or even positive $T$-stress. Analogously to Eq. (2.16), the $T$-stress can be estimated as $T = \hat{t}(a,t)\sigma_{nominal}$ [30], where $\hat{t}(a,t)$ are $T$-stress calibration functions of the specimen under consideration.

Larsson and Carlsson applied boundary tractions corresponding to the stress fields of the first two terms in the Williams eigen expansion of near-tip elastic fields on the same domain as that in the previous BL solution; hence these solutions are termed

*Modified Boundary Layer Solutions (MBL).* Fig. 3.3 compares the plastic zones of actual specimen with those of corresponding MBL solutions at the same value of $K_I$. The MBL solutions using this two-parameter description of the problem are essentially in exact agreement with those of corresponding actual specimen [15].

Recently, extensive work has been done on the two-parameter characterization of near-crack-tip fields. Betegón and Hancock [5] analyzed near-crack-tip fields of plane strain specimens with positive, zero, and negative $T$-stress. The crack-tip opening stress of the actual specimens closely followed the MBL prediction up to large scale yielding. Du and Hancock [7] found that the triaxiality near the crack-tip of a non-hardening material varies with the $T$-stress. Namely, triaxiality decreases with decreasing $T$-stress (see Fig. 3.4). Here $\tau$ is defined as the ratio of the $T$-stress and the tensile yield strength of the material; that is, $\tau = T/\sigma_y$. Wang [31] investigated the influence of the $T$-stress on the crack-tip opening stress in a variety of plane strain $SCP$s. Fig. 3.5 shows the variation of normalized crack-opening stress ($\sigma_{yy}$ at $\theta = 0$) *vs.* normalized distance at various values of $\tau$. The thick solid line at $\tau = 0$ is the stress profile at SSY. The crack-opening stress deviates considerably from the SSY stress with decreasing $\tau$, while the deviation at high positive $\tau$ is less pronounced. From the same study the effect of $T$-stress on the equivalent plastic strain $\bar{\varepsilon}^p$ at a distance from the tip equal to $r = 1.22J/\sigma_y$ is shown in Fig. 3.6. The thick solid line is the SSY solution ($\tau = 0$). Negative $\tau$ is associated with a large increase in $\bar{\varepsilon}^p$ and a shift of the peak to the forward section ($\theta < 90°$). At $\tau = -1.0$, the peak $\bar{\varepsilon}^p$ increases $\sim 80\%$ comparing with the corresponding peak $\bar{\varepsilon}^p$ at $\tau = 0$, and the location of the peak shifts from $\theta \doteq 90°$ at $\tau = 0$ to $\theta \doteq 70°$ at $\tau = -1.0$. A slight decrease of peak $\bar{\varepsilon}^p$ is observed at a $\tau$ value between 0.2 and 0.4. At $\tau = 1.0$, the peak $\bar{\varepsilon}^p$ increases about

25% with respect to the peak value at $\tau = 0$, while the location of the peak at $\tau = 1.0$ shifts back toward the cracked flank by about 20°.

## 3.2 Modified Effective Crack-Length Formulations

The studies of Larsson and Carlsson [15] and Hancock and co-workers ([5]; [2]; [7]) suggest that the plastic zone size is more sensitive to the change of $\tau$ than any other crack-tip parameter. Variation of plastic zone size with $T$-stress was noted by Wang [31]. Fig. 3.7 shows the plastic zone size at various values of $\tau$ normalized by the plastic zone size at $\tau = 0$. More specifically, the ratio of the maximum plastic zone size $r^p_{max}$ to the plastic zone size at $\tau = 0$ is presented on a logarithmic scale. At $\tau = 0$, the calculated $r^p_{max}$ is about $0.15(K_I/\sigma_y)^2$, which slightly differs from the generally used nominal plastic zone size, $r_p = \frac{1}{2\pi}(K_I/\sigma_y)^2$, under plane strain and SSY conditions. The plastic zone size grows monotonically with decreasing $\tau$. At $\tau = -1.0$, the plastic zone size is about 50 times the size at $\tau = 0$. Positive $\tau$ causes the plastic zone size to decrease first, then increase, at $\tau = 1.0$, to about 10 times its size at $\tau = 0$.

Wang [31] furthermore observed a dependence of plastic zone orientation on the $T$-stress. Fig. 3.8 shows the change in orientation of the plastic zone at different values of $\tau$. The zone sizes are normalized by their respective maximum radius, $r_p^{max}$. At negative $\tau$, the plastic zone slightly shifts towards the $\theta = 0°$ line. At positive $\tau$, the plastic zone changes its orientation towards the $\theta = 135°$ line.

Based on this observed sensitivity of plastic zone size and orientation to the sign and magnitude of the $T$-stress, and in analogy with the previous section where the boundary layer solution was modified by the elastic $T$-stress, *Modified Effective Crack Length Formulations* are developed by including the elastic $T$-stress in the effective crack length formulations of Chapter 2. The modified effective crack length can be written in the form

$$a_{eff} = a + r^*_{p,mod} = a + \Lambda(\tau)\left(\frac{K_I}{\sigma_y}\right)^2, \tag{3.2}$$

where $r^*_{p,mod}$ is the plastic zone size correction which depends on the $T$-stress. $\Lambda(\tau)$ is the plastic zone correction factor as a function of $T$-stress. An expression for $r^*_{p,mod}$ was derived by Lee and Parks [16] in their work to enhance the elastic-plastic line-spring finite element by an effective crack length. Their approach is presented in the following.

Referring to Fig. 3.7, the circled data points can be fitted by a fourth-order polynomial. Thus:

$$\hat{e}(\tau) \equiv \log \frac{r^p_{max}(\tau)}{r^p_{max}|_{\tau=0}} \doteq c_1\tau + c_2\tau^2 + c_3\tau^3 + c_4\tau^4, \tag{3.3}$$

where $(c_1, c_2, c_3, c_4) = (-0.539, 0.375, 0.236, 0.974)$ are fitting coefficients.

A first approximation to the correction part of the effective crack length $r^*_{p,mod}$ is obtained by assuming

$$r^*_{p,mod} = r^p_{max}(\tau) = r^p_{max}|_{\tau=0} \times \frac{r^p_{max}(\tau)}{r^p_{max}|_{\tau=0}}. \tag{3.4}$$

Using the ratio expression in Eq. (3.3) and noting that $r^p_{max}|_{\tau=0} = 0.15\,(\frac{K_I}{\sigma_y})^2$, $r^*_{p,mod}$ can be witten as

$$r^*_{p,mod} = 0.15 \times 10^{\hat{e}(\tau)} \times (\frac{K_I}{\sigma_y})^2. \tag{3.5}$$

This first-order estimate is based on a maximum plastic zone size. However, in plane strain the maximum size of the plastic zone (at angles $\theta > 45°$) is a large multiple of the size of the plastic zone immediately ahead of the crack tip ($\theta = 0$) (see Fig. 3.9). Thus a correction of the first-order estimate in Eq. (3.5) has to be determined. Lee and Parks determined this correction, which they termed $\beta$, as 0.12 by comparing their numerical results (tensile load $N$ *vs.* cracked displacement $\delta^c$ or $J$-integral $J$ *vs.* $\delta^c$) for a $SEN$ specimen of relative crack depth $a/t = 0.5$ with the elastic-plastic FE solution of the same specimen and by "tuning" $\beta$ until good agreement with the continuum solution was found. Fig. 3.10 shows a graph of load $N$ *vs.* $\delta^c$ for the $SEN$ specimen at various values of $\beta$ (ranging from $\beta = 0$ to $\beta = 0.24$ in increments of 0.06).

Incorporating this correction in Eq. (3.5), a second-order estimate of the modified plastic-zone correction is obtained as

$$r^*_{p,mod} = 0.12 \times 0.15 \times 10^{\hat{e}(\tau)} \times (\frac{K_I}{\sigma_y})^2 = 0.018 \times 10^{\hat{e}(\tau)} \times (\frac{K_I}{\sigma_y})^2. \tag{3.6}$$

Thus, the modified effective crack length can be written as

$$a_{eff} = a + 0.018 \times 10^{\hat{e}(\tau)} \times \left(\frac{K_I(a_{eff}, t)}{\sigma_y}\right)^2. \tag{3.7}$$

It is to be noticed that for $\tau = 0$, Eq. (3.7) reduces to the effective crack length formulation of Chapter 2 (Eq. (2.15)). The corresponding plastic zone correction factor (A = 0.018) is almost identical to the Edmunds and Willis correction factor for an elastic-perfectly plastic material satisfying the Mises yield criterion (see Eq. (2.14)).

To evaluate $\hat{e}(\tau)$ in Eq. (3.7), $\tau$ can be estimated as

$$\tau = \frac{T(a,t)}{\sigma_y} = \hat{t}(a,t)\frac{\sigma_{nominal}}{\sigma_y}, \tag{3.8}$$

where $\hat{t}(a,t)$ are $T$-stress calibration functions of the specimen under consideration. Sham ([25]; [26]) has tabulated the $\hat{t}(a,t)$ using second-order weight functions for various specimens for essentially the entire range of $a/t$. Fig. 3.11 shows the variation of $\hat{t}(a,t)$ in terms of the relative crack depth for the $SEN$ specimen in remote tension. The variation of $\hat{t}(a,t)$ for the $CCP$ and $DEN$ are shown in Figs. 3.12 and 3.13.

Introduction of an effective crack length instead of the actual crack length makes $\tau$ a function of $a_{eff}$, that is

$$\tau = \frac{T(a_{eff}, t)}{\sigma_y} = \hat{t}(a_{eff}, t)\frac{\sigma_{nominal}}{\sigma_y}. \tag{3.9}$$

To use $\hat{t}(a,t)$ in Eq. (3.9), Wang [31] fitted the data points for the $SEN$ specimen shown in Fig. 3.11 in the range of $0.1 \leq a/t \leq 0.8$ with a fourth-order polynomial function, yielding:

$$\hat{t}_{SEN}(a_{eff},t) = a_o + a_1(\frac{a_{eff}}{t}) + a_2(\frac{a_{eff}}{t})^2 + a_3(\frac{a_{eff}}{t})^3 + a_4(\frac{a_{eff}}{t})^4, \qquad (3.10)$$

where $(a_o, a_1, a_2, a_3, a_4) = (-0.211, -5.86, 31.8, -74.9, 65.6)$ for $\hat{t}_{SEN}$ in tension. Linear variations were assumed for $0 < a/t < 0.1$ with $\hat{t}_{SEN}(a_{eff},t) = -0.54$ at $a/t = 0$ [5].

In the same way, the data points for the $CCP$ specimen (Fig. 3.12) were fitted in the range of $0 \leq a/t \leq 0.8$ with a fifth-order polynomial function:

$$\hat{t}_{CCP}(\frac{a_{eff}}{t}) = a_o + a_1(\frac{a_{eff}}{t}) + a_2(\frac{a_{eff}}{t})^2 + a_3(\frac{a_{eff}}{t})^3 + a_4(\frac{a_{eff}}{t})^4 + a_5(\frac{a_{eff}}{t})^5, \quad (3.11)$$

where $(a_o, a_1, a_2, a_3) = (-1.0, -0.305, 2.816, -15.539, 28.455, -20.937)$. The value $a_o = -1.0$ at $a_{eff}/t = 0$ corresponds to the analytical result for a Griffith crack under uniaxial tension, that is, $T = \hat{t}(a_{eff},t)|_{\frac{a_{eff}}{t}=0} \times \sigma^{nominal} = -\sigma^{nominal}$.

Data points for the $DEN$ specimen were fitted with a third-order polynomial in the range $0.1 \leq a/t \leq 0.9$ (Fig. 3.13),

$$\hat{t}_{DEN}(a_{eff},t) = a_o + a_1(\frac{a_{eff}}{t}) + a_2(\frac{a_{eff}}{t})^2 + a_3(\frac{a_{eff}}{t})^3, \qquad (3.12)$$

To use $\hat{t}(a,t)$ in Eq. (3.9), Wang [31] fitted the data points for the $SEN$ specimen shown in Fig. 3.11 in the range of $0.1 \leq a/t \leq 0.8$ with a fourth-order polynomial function, yielding:

$$\hat{t}_{SEN}(a_{eff},t) = a_o + a_1(\frac{a_{eff}}{t}) + a_2(\frac{a_{eff}}{t})^2 + a_3(\frac{a_{eff}}{t})^3 + a_4(\frac{a_{eff}}{t})^4, \qquad (3.10)$$

where $(a_o,a_1,a_2,a_3,a_4) = (-0.211,-5.86,31.8,-74.9,65.6)$ for $\hat{t}_{SEN}$ in tension. Linear variations were assumed for $0 < a/t < 0.1$ with $\hat{t}_{SEN}(a_{eff},t) = -0.54$ at $a/t = 0$ [5].

In the same way, the data points for the $CCP$ specimen (Fig. 3.12) were fitted in the range of $0 \leq a/t \leq 0.8$ with a fifth-order polynomial function:

$$\hat{t}_{CCP}(\frac{a_{eff}}{t}) = a_o + a_1(\frac{a_{eff}}{t}) + a_2(\frac{a_{eff}}{t})^2 + a_3(\frac{a_{eff}}{t})^3 + a_4(\frac{a_{eff}}{t})^4 + a_5(\frac{a_{eff}}{t})^5, \quad (3.11)$$

where $(a_o,a_1,a_2,a_3,a_4,a_5) = (-1.0,-0.305,2.816,-15.539,28.455,-20.937)$. The value $a_o = -1.0$ at $a_{eff}/t = 0$ corresponds to the analytical result for a Griffith crack under uniaxial tension, that is, $T = \hat{t}(a_{eff},t)|_{\frac{a_{eff}}{t}=0} \times \sigma^{nominal} = -\sigma^{nominal}$.

Data points for the $DEN$ specimen were fitted with a third-order polynomial in the range $0.1 \leq a/t \leq 0.9$ (Fig. 3.13),

$$\hat{t}_{DEN}(a_{eff},t) = a_o + a_1(\frac{a_{eff}}{t}) + a_2(\frac{a_{eff}}{t})^2 + a_3(\frac{a_{eff}}{t})^3, \qquad (3.12)$$

where $(a_o, a_1, a_2, a_3) = (-0.525, 0.01, -0.212, 0.122)$.

In summary, an expression for $a_{eff}$ has been developed (see Eq. (3.2)) which through the stress intensity factor $K_I$ and through the elastic $T$-stress depends on $a_{eff}$ implicitly. For given values of $N$, Eq. (3.2) has been solved numerically using the Newton-Raphson method. In analogy with Chapter 2, the corresponding values of $J(a_{eff}, t)$ and $\delta^c(a_{eff}, t)$ were determined using Eqs. (2.17) and (2.22). Curves of $N$ *vs.* $\delta^c$ and $N$ *vs.* $J$ were generated for the $SEN$, $CCP$, and $DEN$ specimens at relative crack depths $a/t = 0.5, 0.35,$ and $0.2$ and compared to the corresponding curves of Chapter 2.

## 3.3 Results and Discussion

Curves of normalized load *vs.* cracked displacement of the three specimens are shown in Figs. 3.15, 3.18, and 3.21. Figs. 3.17, 3.20, and 3.23 show normalized values of $J$ *vs.* load $N$. Figs. 3.16, 3.19, and 3.22 show the evolution of the modified effective crack lengths of the three specimens with increasing load. LEFM solutions and solutions based on the effective crack length formulation of Chapter 2 (Eq. (2.15)) are shown for the purpose of comparison. The method of Chapter 2 was used to determine the load levels at which deviation from the continuum solution occurs. Solutions based on effective crack length formulations and on modified effective crack length formulations are compared.

For the $SEN$ specimen, use of a modified effective crack length extends the load range of accurate solution by approximately 25% of limit load for the cracks of length

0.2 and 0.35 and by approximately 12% for the crack of length 0.5. Load ranges of accurate solution for the $CCP$ specimen are increased by approximately 15% for the 0.2 crack and by 21% and 24% for the 0.35 and 0.5 crack, respectively. Increases in load range for the $DEN$ specimen go from 24% for the 0.2 crack to 30% for the 0.5 crack. The load range of accurate solution for the 0.35 crack is increased by $\sim 29\%$ compared to the effective crack length solution of Chapter 2.

Thus, inclusion of the $T$-stress in the standard effective crack length formulation significantly extends the load ranges of accurate solutions of all specimens. More important than this, however, is the qualitative behavior of the $T$-stress modified curves. The $T$-stress allows the solutions based on modified effective crack lengths to separate from the LEFM and the plastically corrected solutions and to follow the continuum solution into the regime of elastic-plastic transition. This influence of the $T$-stress seems to be more beneficial for the $SEN$ and $DEN$ specimens than for the $CCP$ specimen. The elastic-plastic transition is followed very accurately for the $SEN$ specimen of all relative crack depths (see Fig. 3.15). In the case of the $DEN$ specimen, the continuum solution is followed only in the initial part of the elastic-plastic transition region. The $T$-stress influence is not strong enough and soon deviates from the continuum solution (Fig. 3.21). On the other hand, the modified solutions of the $CCP$ specimen overcorrect due to the $T$-stress (Fig. 3.18). Here, the $T$-stress causes the modified solutions to separate from the LEFM and the plastically corrected solutions prematurely. For the $CCP$ specimen of relative crack depth 0.2 this overcorrection is more severe than in the case of the $CCP$ specimen of relative crack depth 0.5.

This varying influence of the $T$-stress with specimen type and relative crack depth can be explained by evaluating $\tau$ for the three specimens at a fixed load level corresponding to a fraction of respective limit load at varying crack depth. A graph of $\tau$ at 75% of limit load is shown in Fig. 3.14.

Values of $\tau$ for the $CCP$ specimen are the most negative of the three specimens and range from $-0.71$ for the 0.2 crack to $-0.54$ for the crack of length 0.5. Values of $\tau$ for the $SEN$ and $DEN$ specimens are almost equal for the crack of length 0.2 ($\tau \sim -0.41$). In the case of the $SEN$ specimen, $\tau$ becomes rapidly less negative as the crack length increases to 0.5 while for the $DEN$ specimen only a slight increase to a value of $\tau = -0.33$ at $a/t = 0.5$ can be noted. This observed change in magnitude with relative crack depth suggests that the overcorrecting influence becomes more severe as $\tau$ becomes more negative. This observation is consistent with the observed decrease of triaxiality with decreasing values of $\tau$. Moderate negative values of $\tau$ help to loosen the crack-tip constraint by decreasing the level of triaxiality (see Fig. 3.4) and thus increase the plastic zone correction of the effective crack length. Conversely, if $\tau$ becomes too negative, a level of triaxiality is reached such that the plastic zone correction is no longer beneficial.

In summary, it has been shown that the elastic $T$-stress consistently extends the range of validity of effective crack length formulations in the analyzed specimen geometries. The magnitude of influence of the $T$-stress varies with specimen type and relative crack depth. The greatest improvement to standard effective crack length approximations occurs in specimens of "moderately" negative $T$-stress.

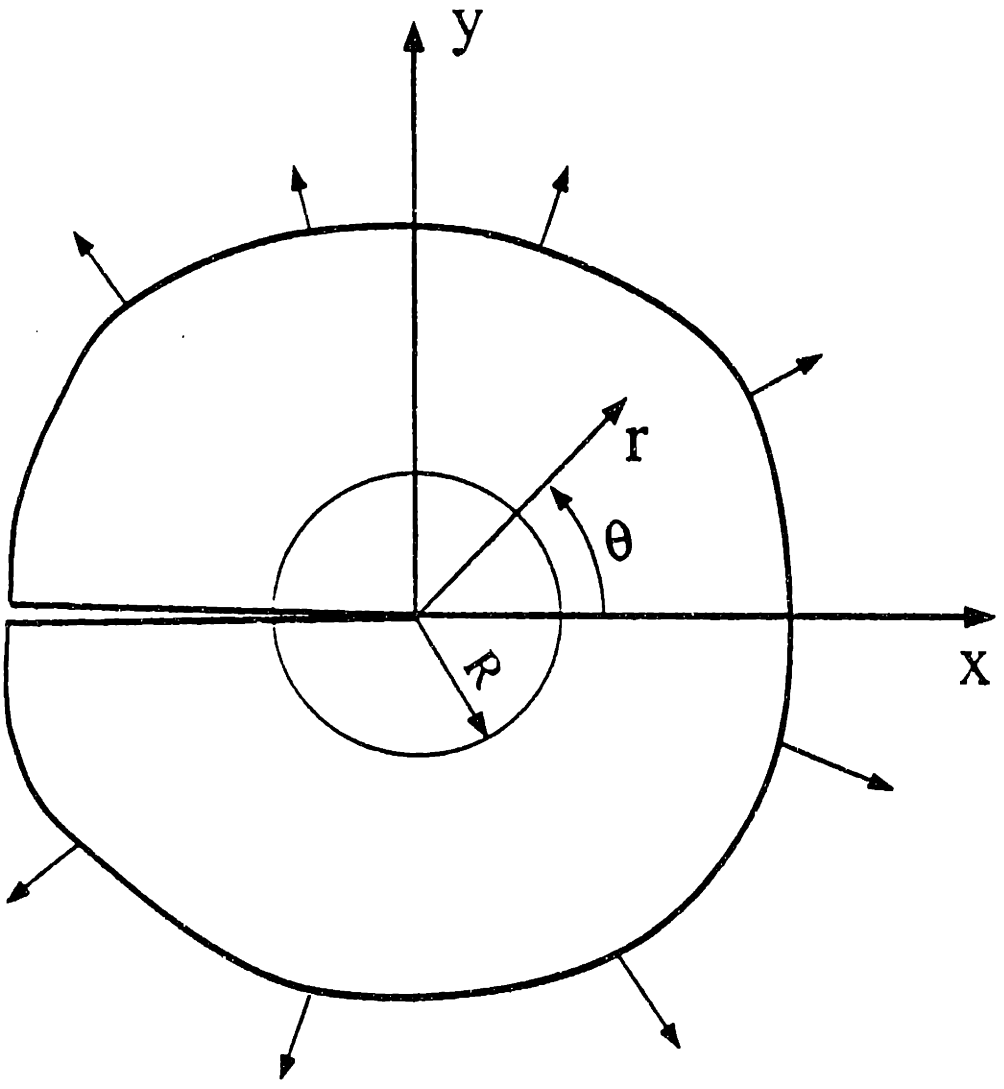


Figure 3.1: Near-crack-tip representation for boundary layer approach [31].

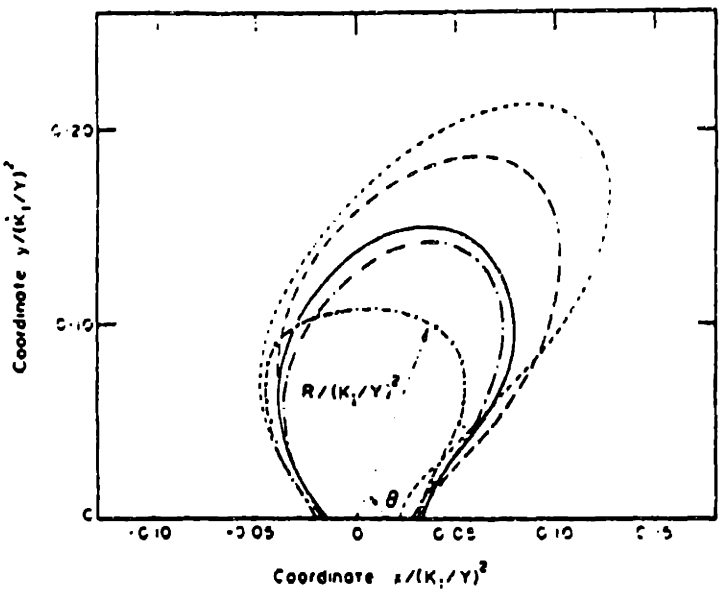


------ Center-cracked specimen

– – – – Double-edge-cracked specimen

—·—·— Bend specimen

*– – –* Compact tension specimen

——— Boundary layer solution

Figure 3.2: Plastic zones in a coordinate system, non-dimensionalized with respect to the characteristic length parameter $(K_I/Y)^2$, of various specimens and BL solution at $K_I = 0.6\,Y\,a^{1/2}$ [15].

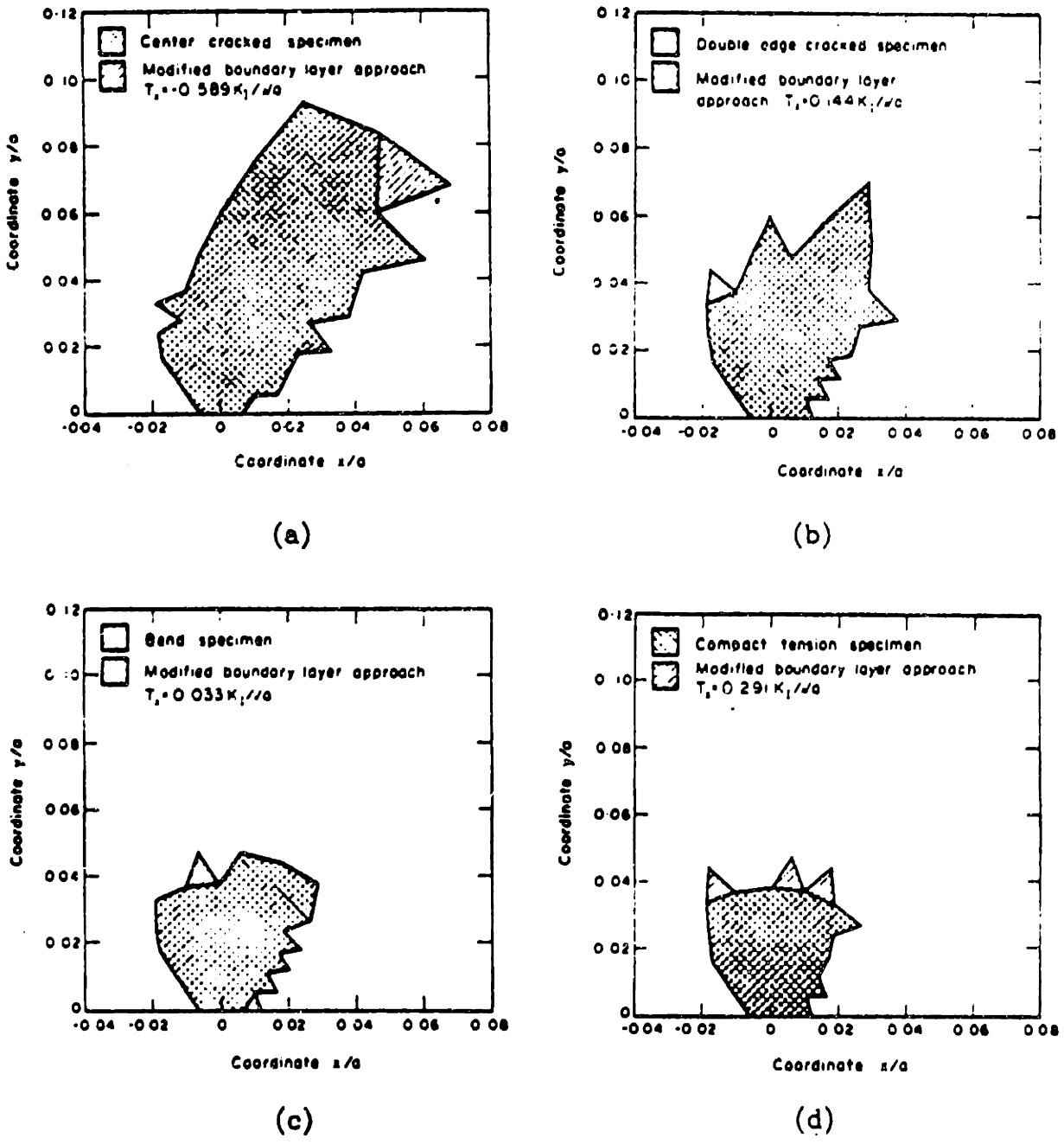


Figure 3.3: Plastic Zones at a load level $K_I = 0.6\,Y\,a^{1/2}$ for actual geometries and for corrected boundary-value solution [15].

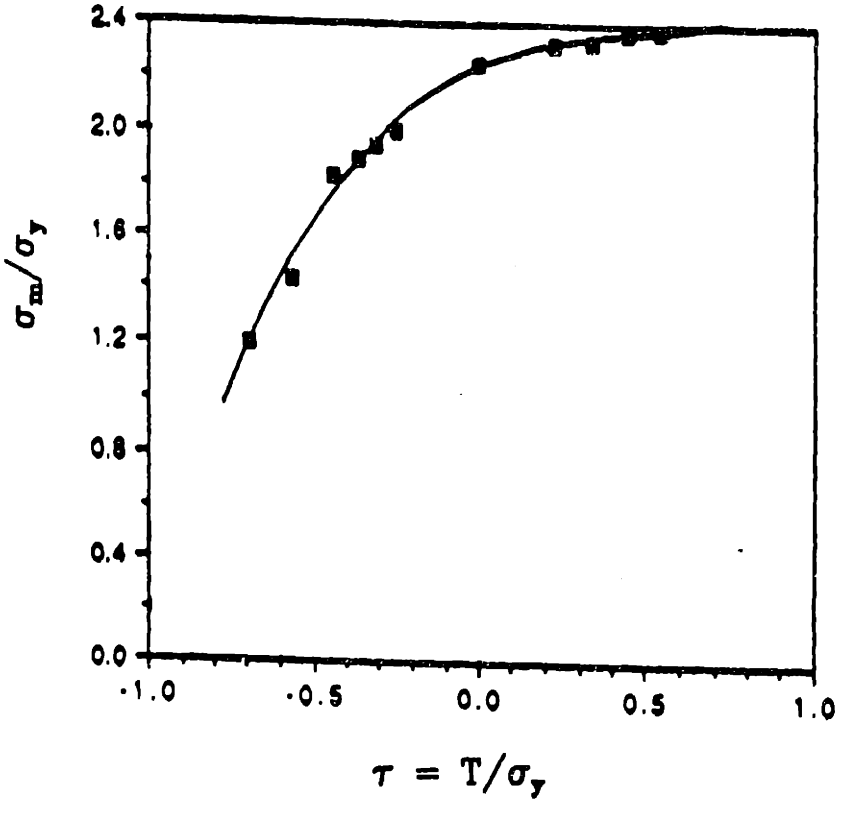


Figure 3.4: The variation of stress triaxiality near a crack tip with respect to $\tau$ in a nonhardening material [7].

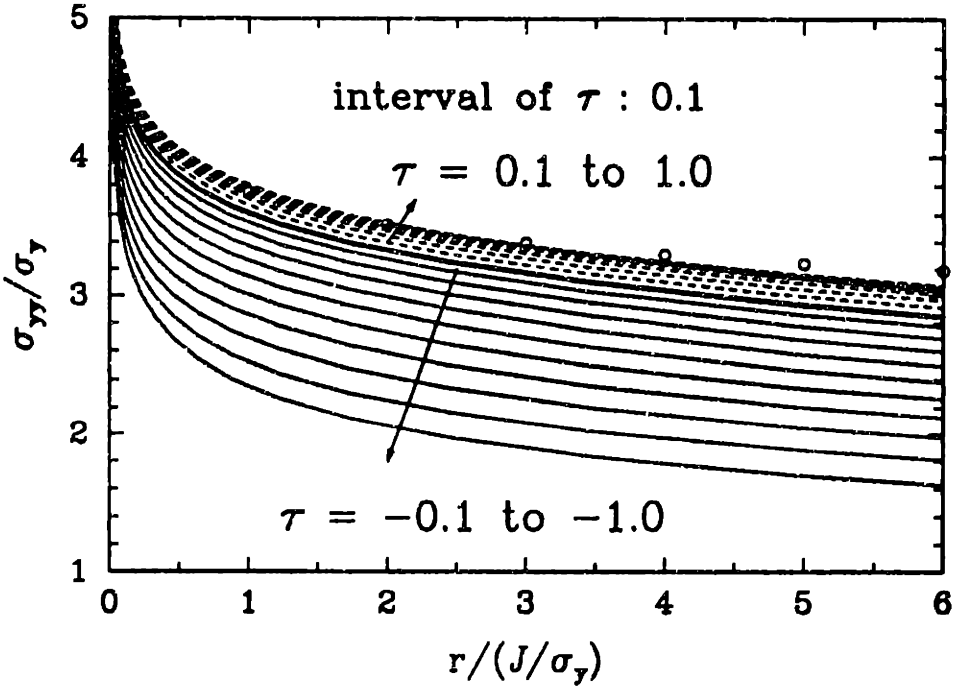


Figure 3.5: Normalized crack opening stress profiles at various values of $\tau$. The stresses marked with circles are HRR-singularity fields [31].

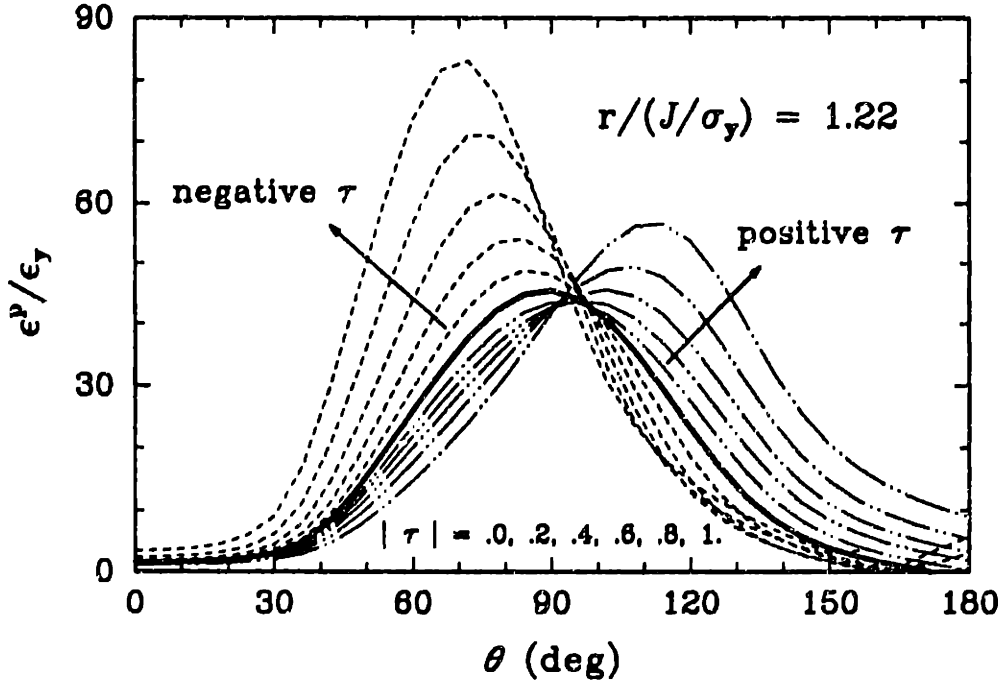


Figure 3.6: Variation of equivalent plastic strain at various $\tau$ [31].

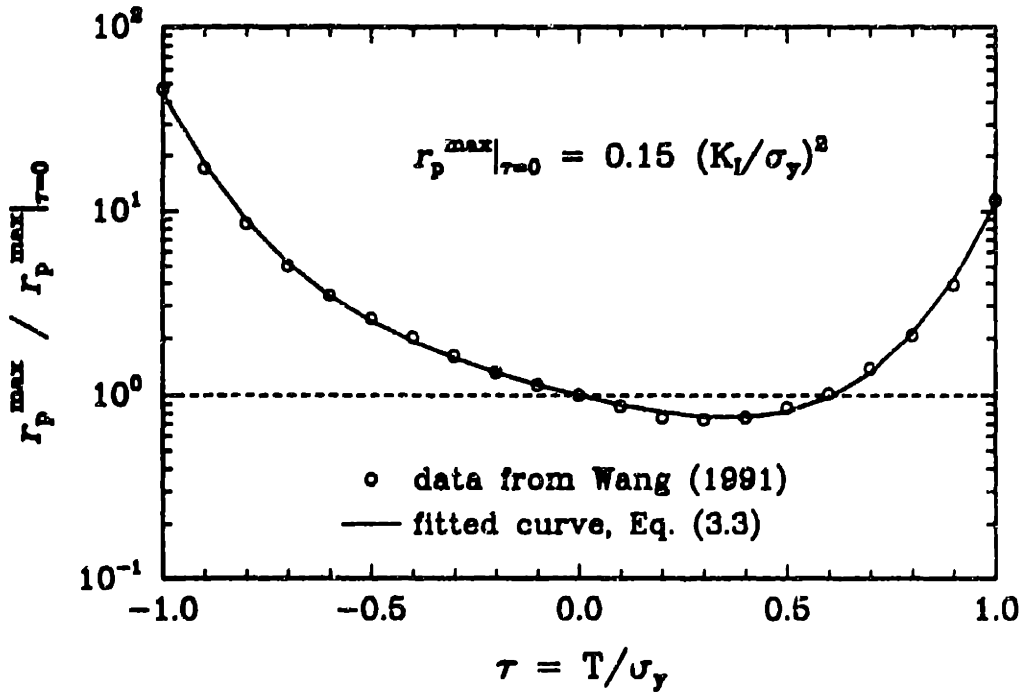


Figure 3.7: Variation of equivalent plastic zone size normalized by the plastic zone size at $\tau = 0$ at various values of $\tau$ ([31]; [16]).

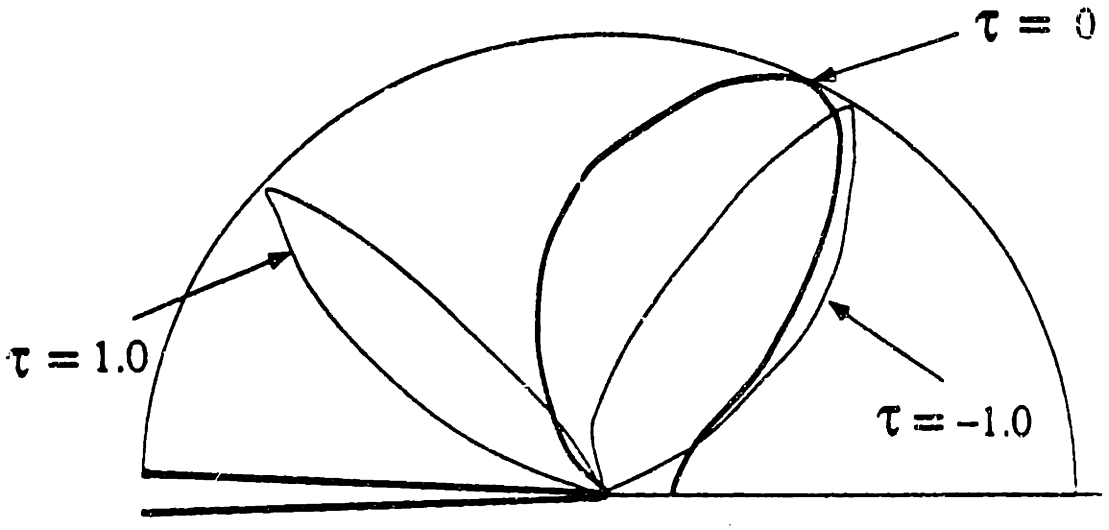


Figure 3.8: Schematic of the plastic zone orientation change at various values of $\tau$. All dimensions of the plastic zone are normalized by the maximum radius of the respective plastic zone [31].

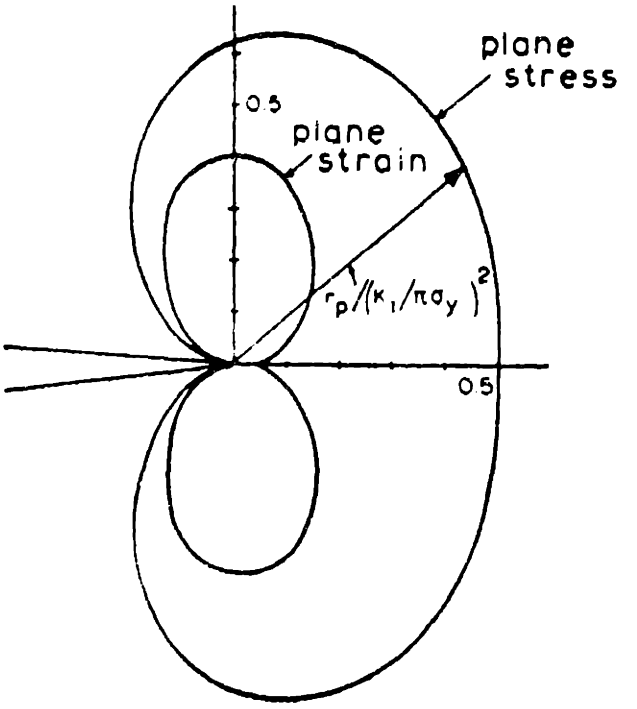


Figure 3.9: Approximate plastic zone shapes according to the von Mises yield criterion applied to the elastic crack-tip stress field [6].

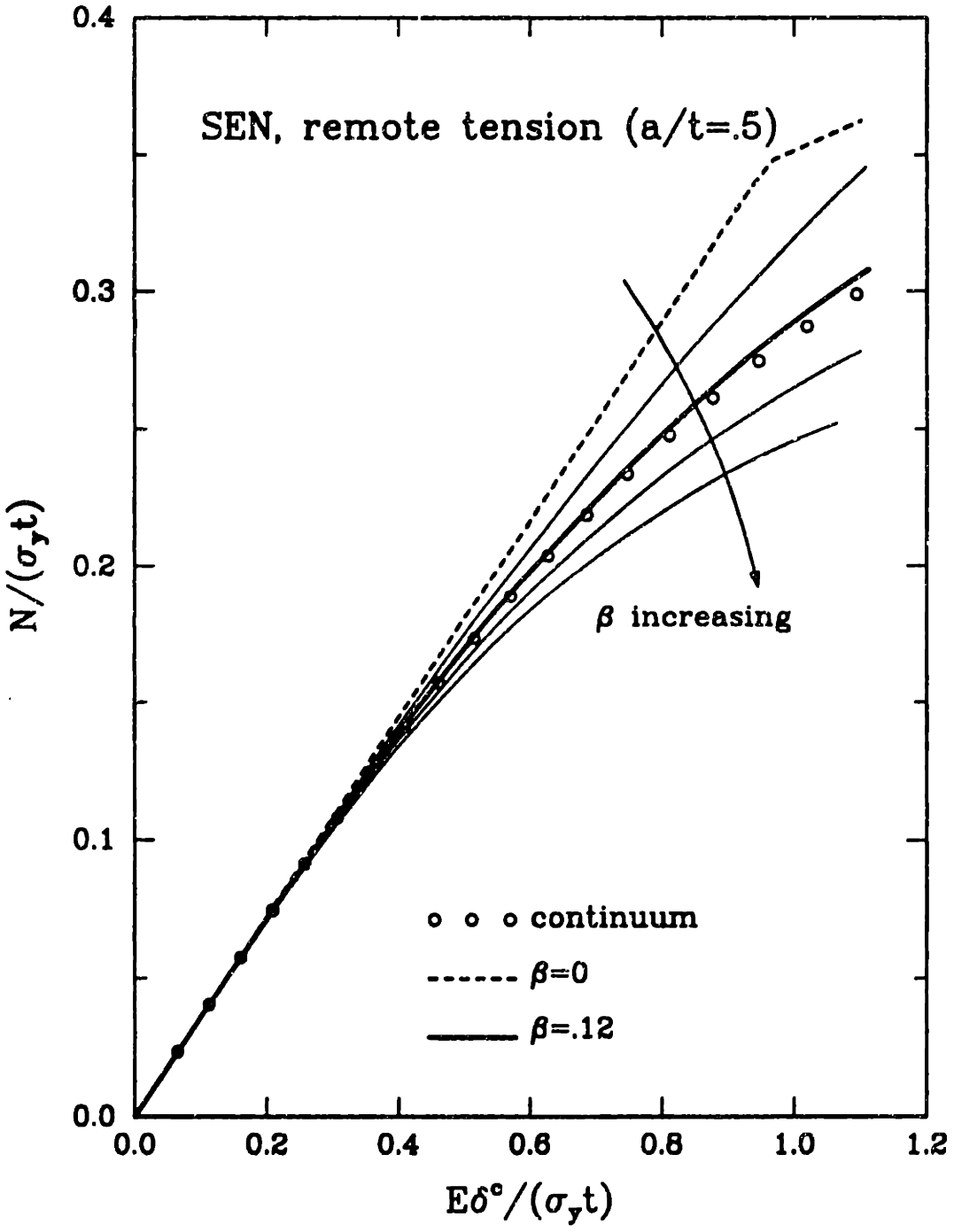


Figure 3.10: Normalized axial force $N$ *vs.* cracked displacement $\delta^c$ of a plane strain $SEN$ of relative crack depth $a/t = 0.5$ under tension. Good agreement between numerical and continuum solution is found for $\beta = 0.12$ [16].

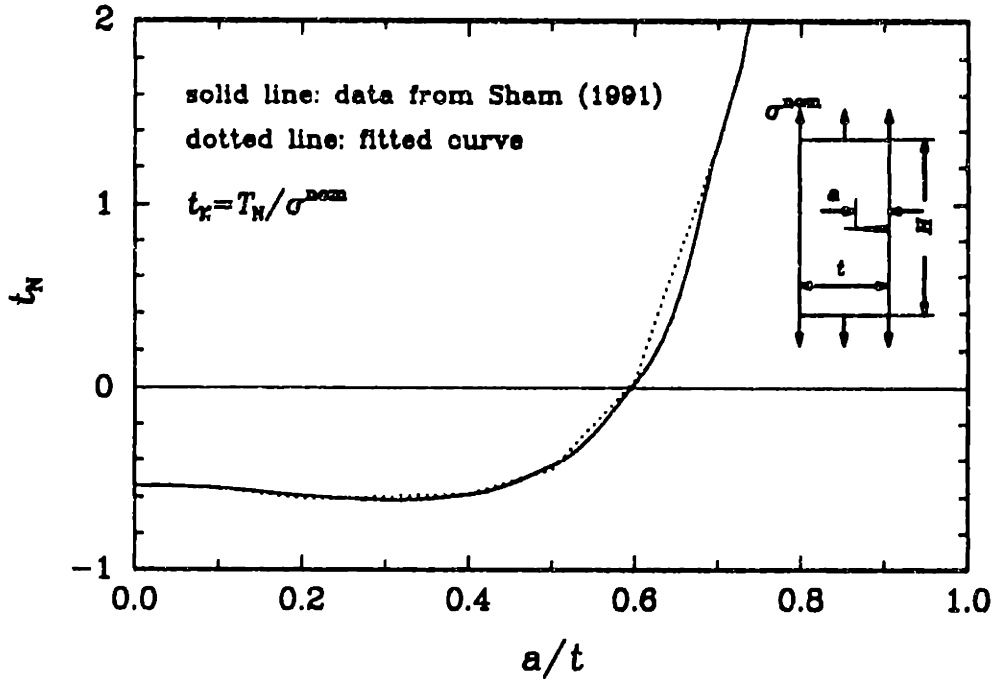


Figure 3.11: $T$-stress calibration function of single edge-cracked specimen under tension [31].

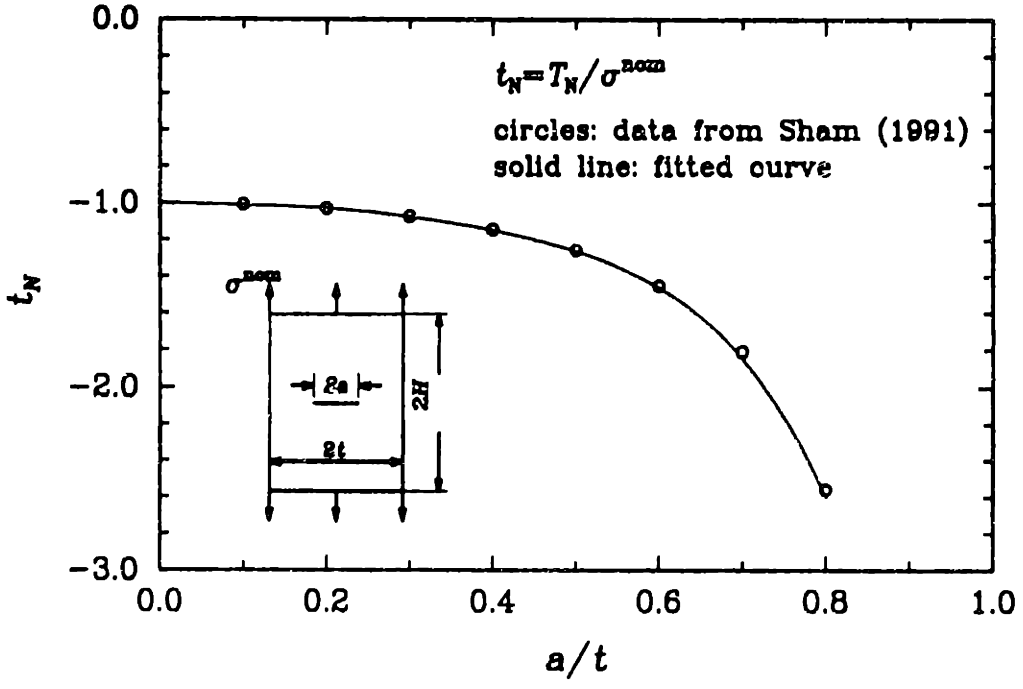


Figure 3.12: $T$-stress calibration function of center-cracked specimen under tension [26].

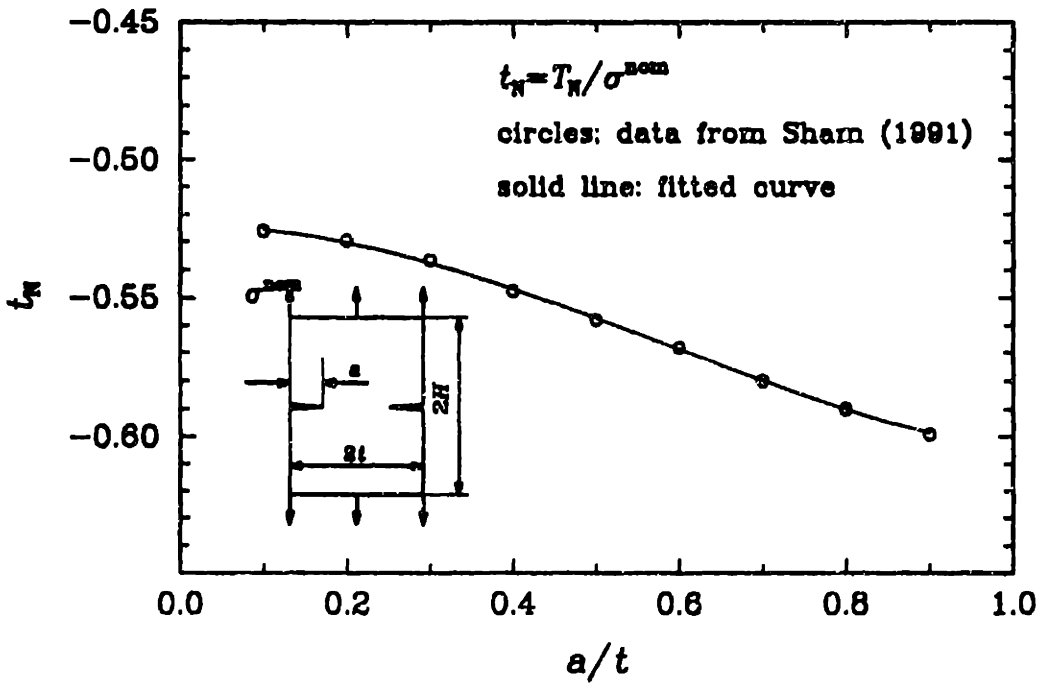


Figure 3.13: $T$-stress calibration function of double edge-cracked specimen under tension [26].

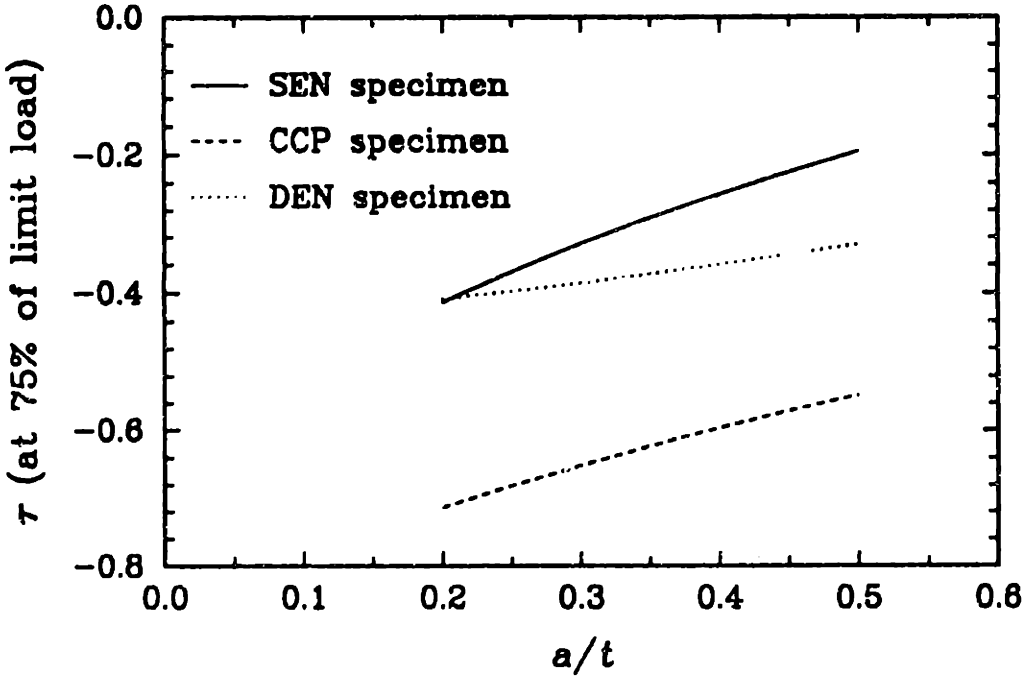


Figure 3.14: Variation of $\tau$ at 75% of limit load for the $SEN$, $CCP$, and $DEN$ specimens.

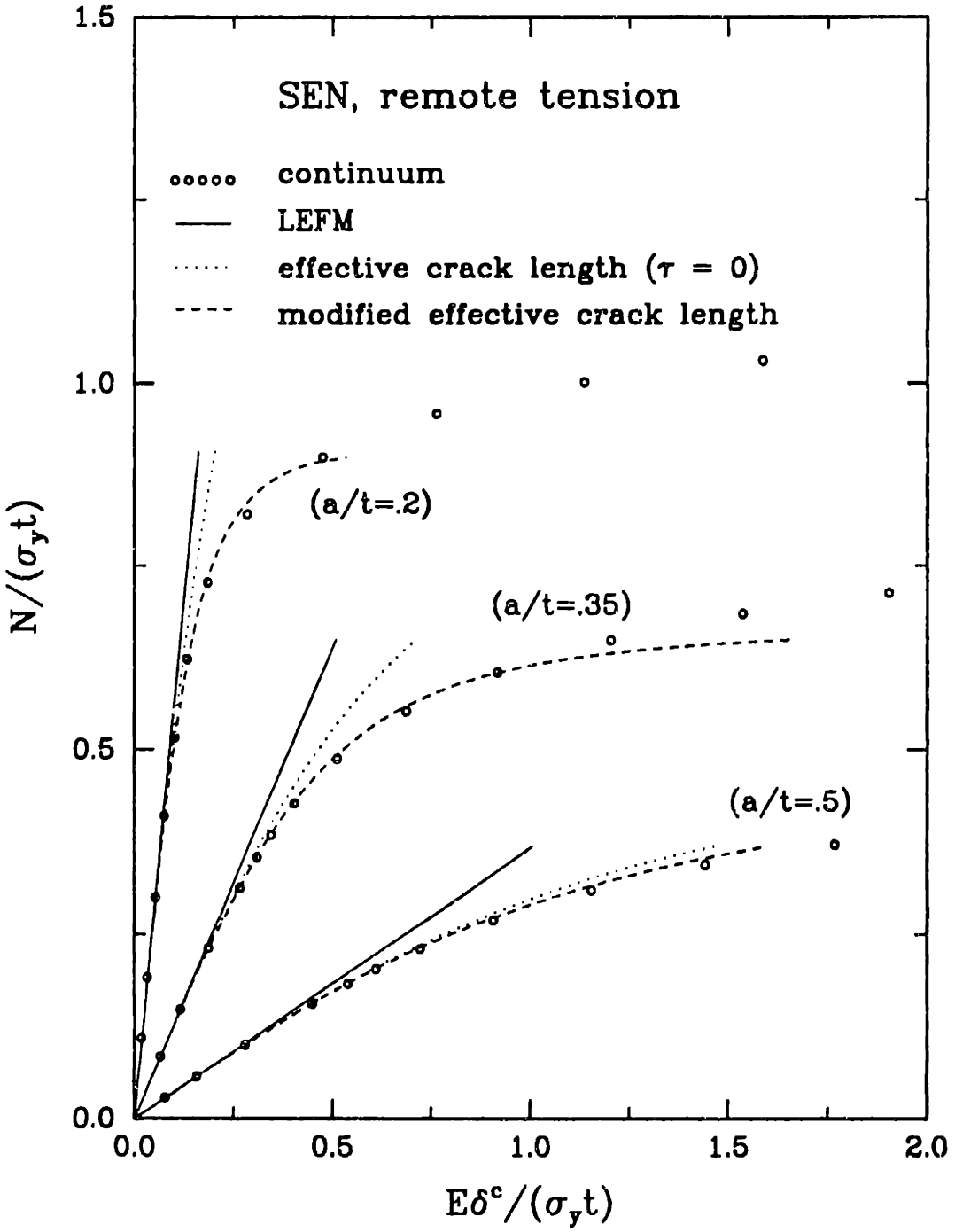


Figure 3.15: Normalized axial force $N$ *vs.* cracked displacement for remote tension of a plane strain $SEN$.

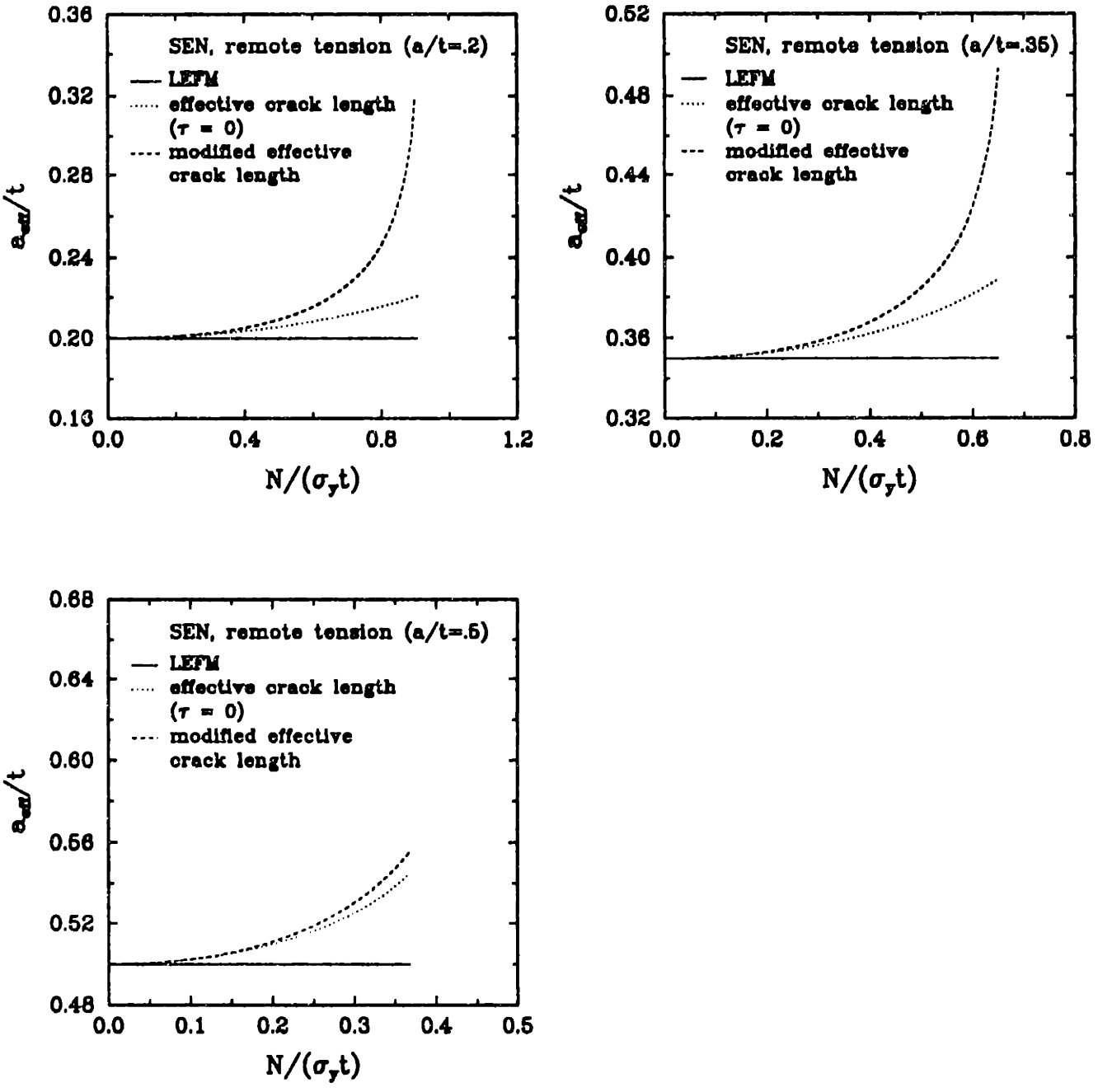


Figure 3.16: Normalized effective crack length *vs.* axial force $N$ for remote tension of a plane strain $SEN$.

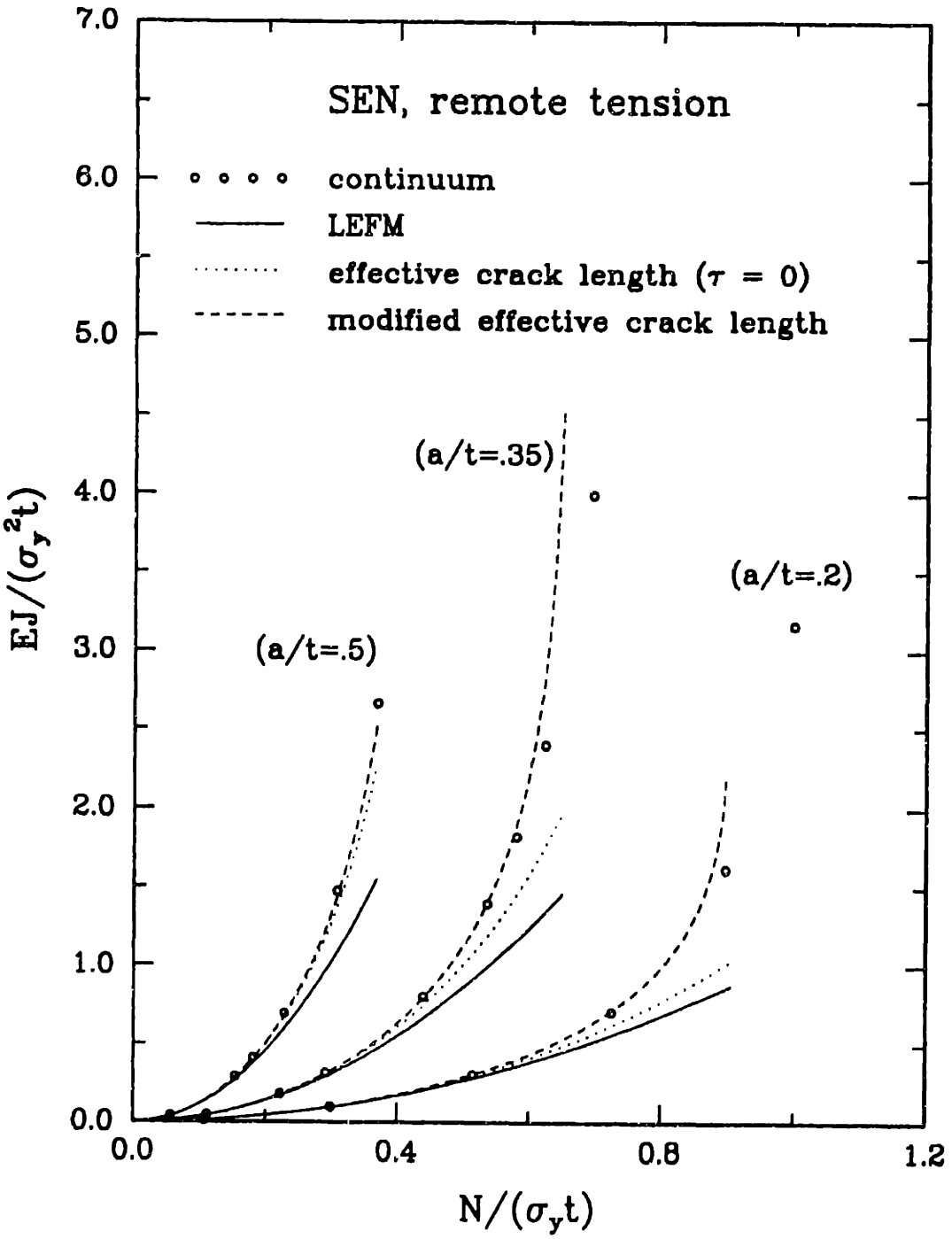


Figure 3.17: Normalized $J$ *vs.* axial force $N$ for remote tension of a plane strain *SEN*.

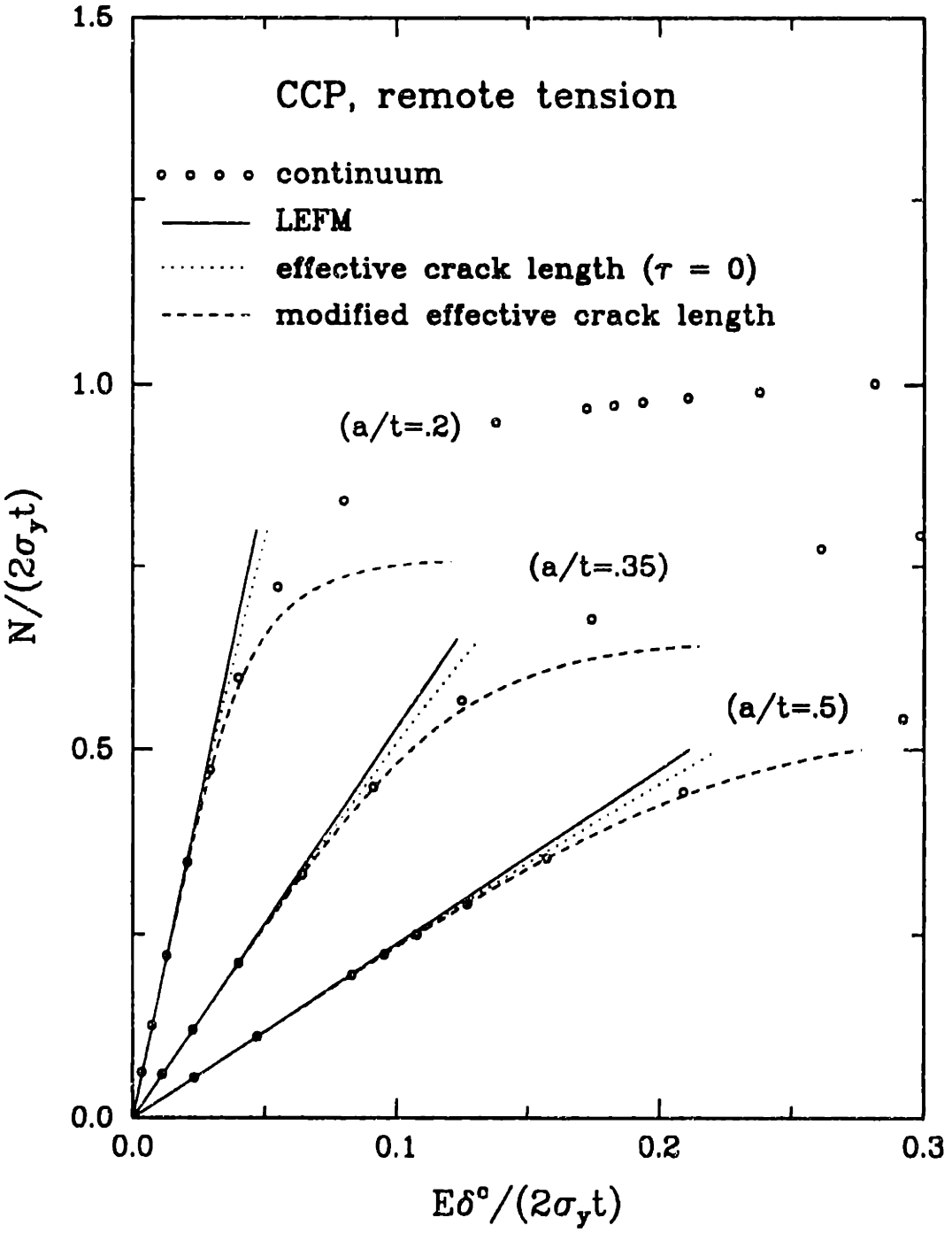


Figure 3.18: Normalized axial force $N$ *vs.* cracked displacement for remote tension of a plane strain $CCP$.

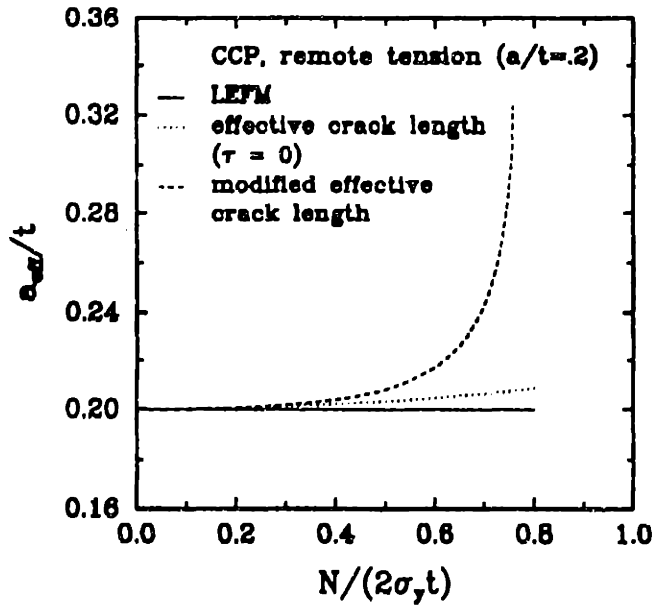


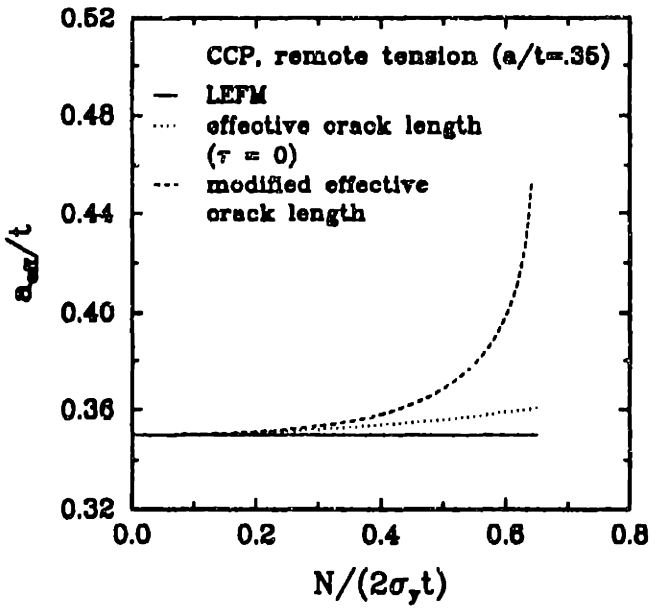


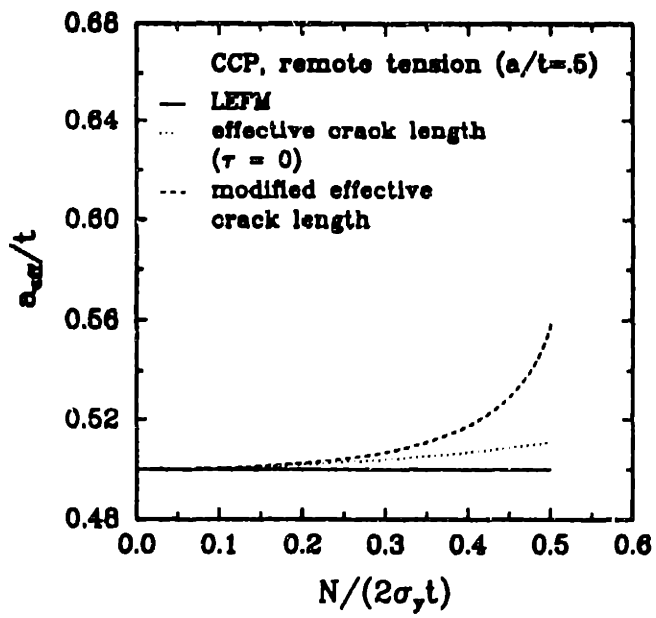


Figure 3.19: Normalized effective crack length *vs.* axial force $N$ for remote tension of a plane strain $CCP$.

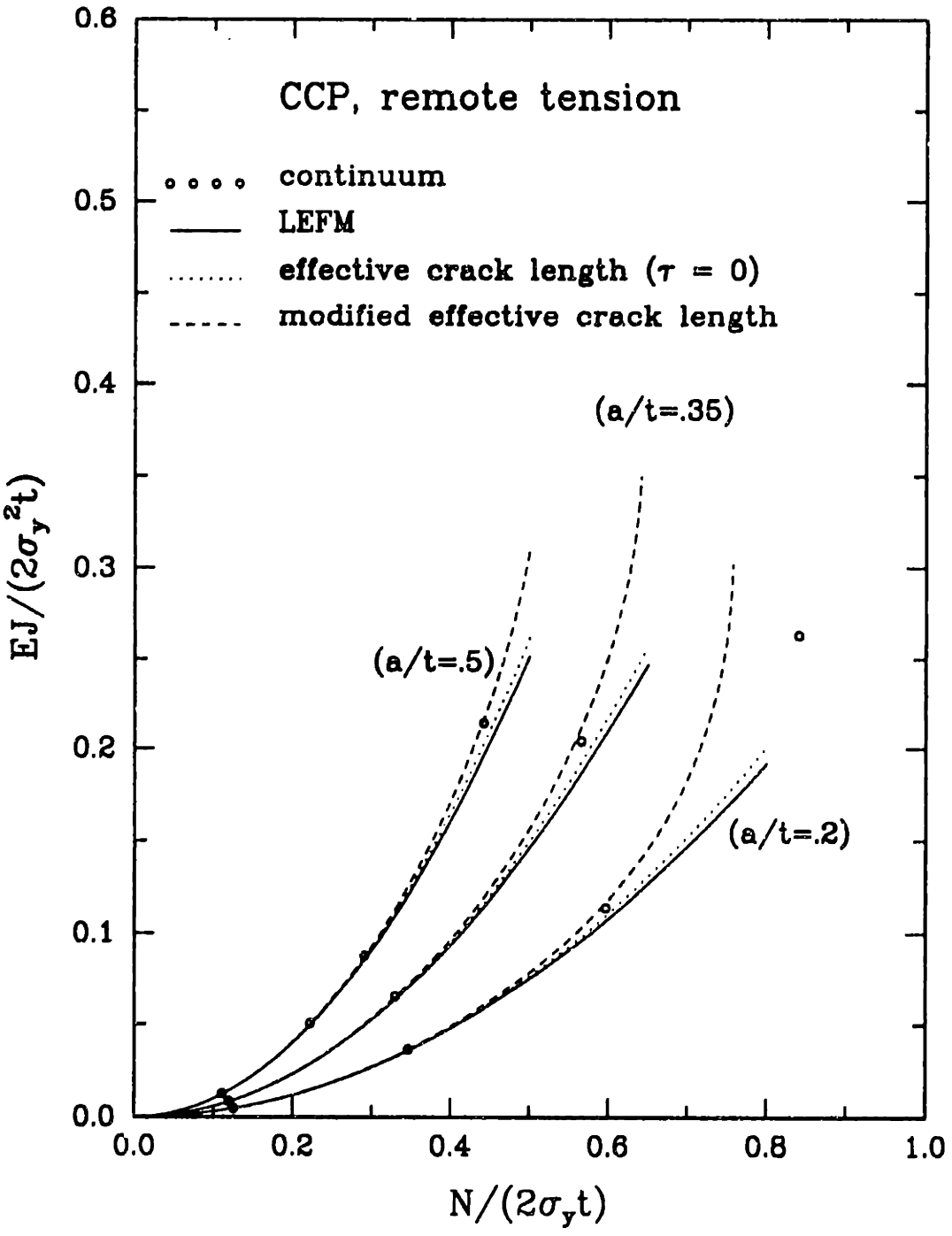


Figure 3.20: Normalized $J$ *vs.* axial force $N$ for remote tension of a plane strain *CCP*.

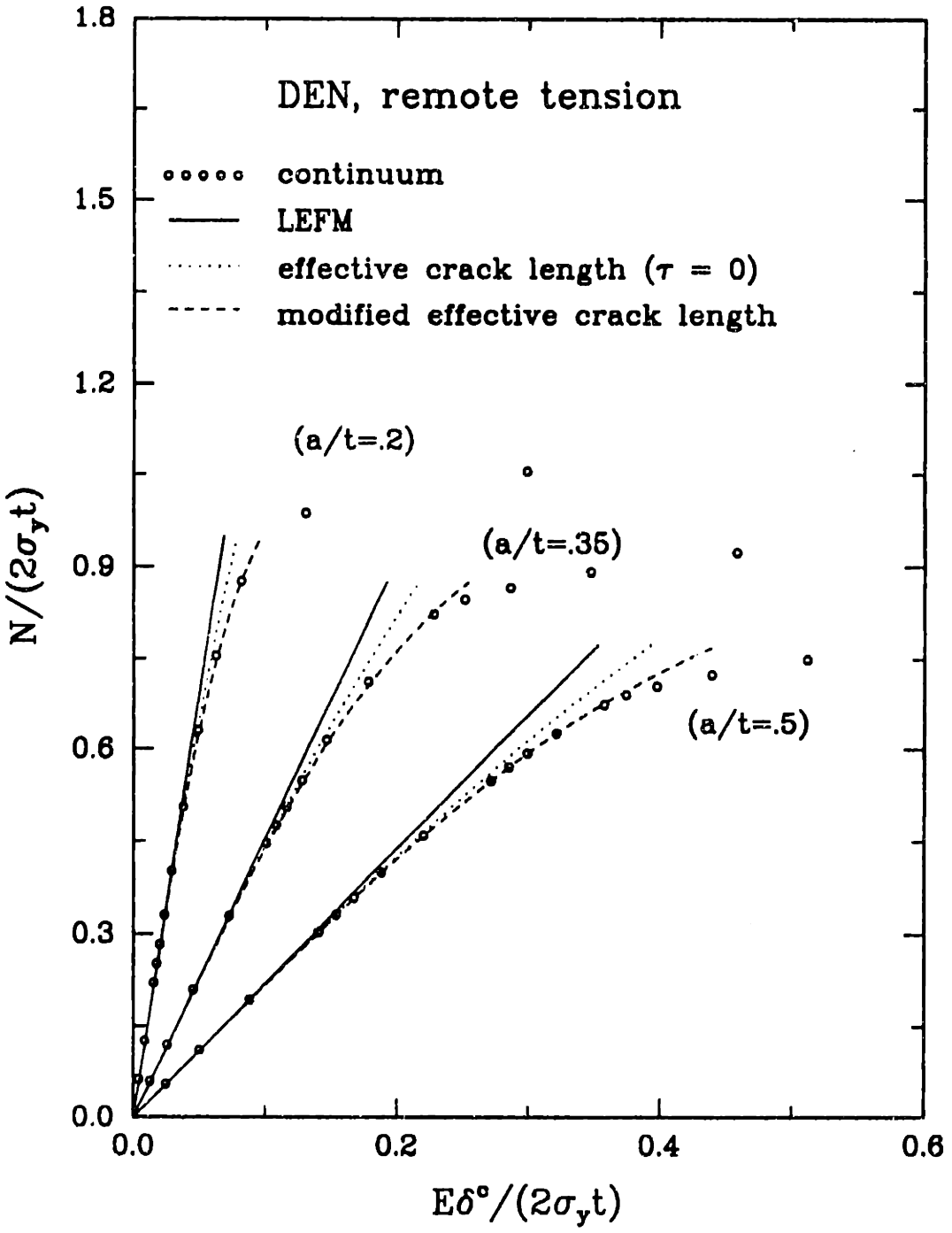


Figure 3.21: Normalized axial force $N$ *vs.* cracked displacement for remote tension of a plane strain *DEN*.

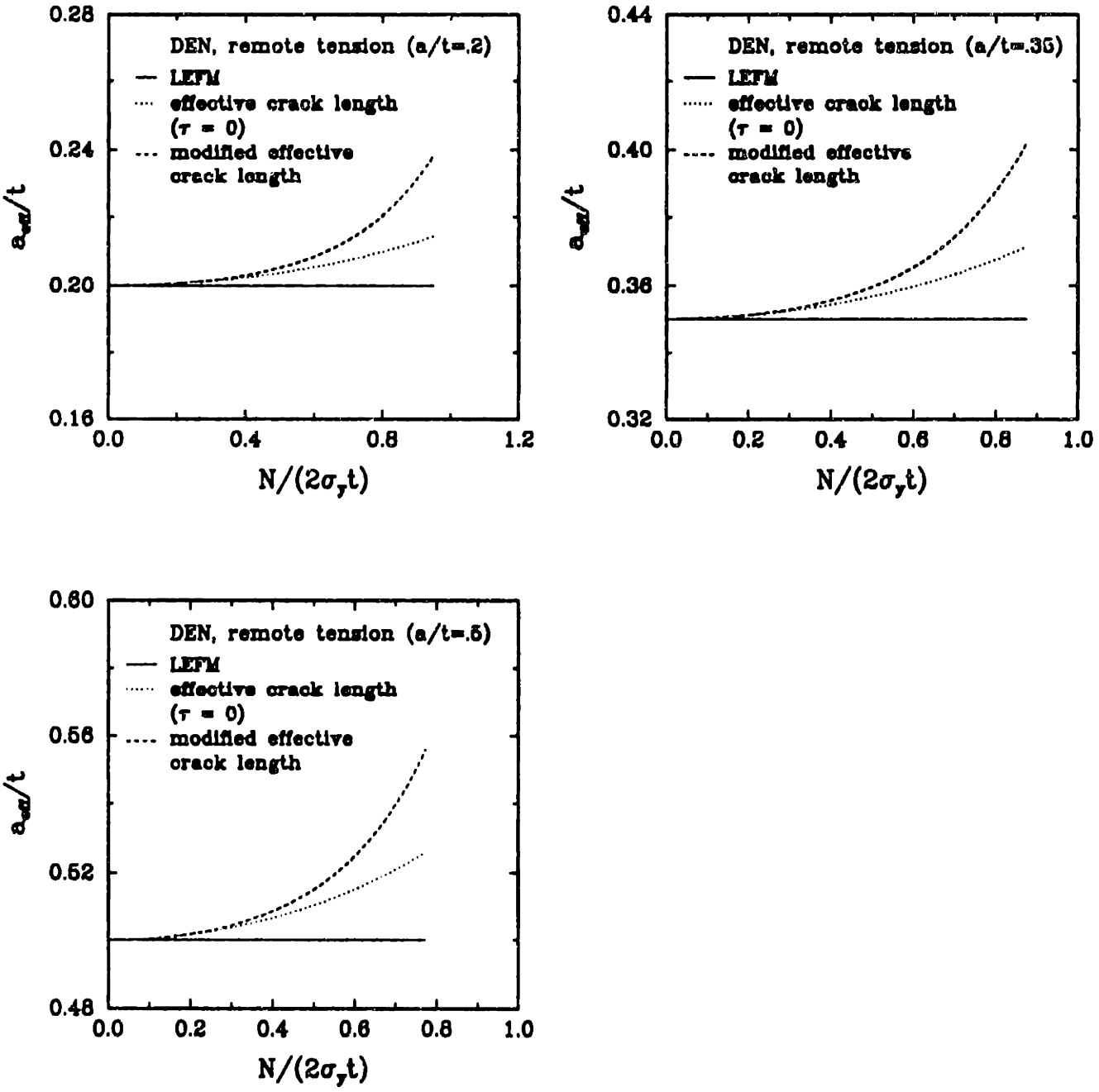


Figure 3.22: Normalized effective crack length *vs.* axial force $N$ for remote tension of a plane strain *DEN*.

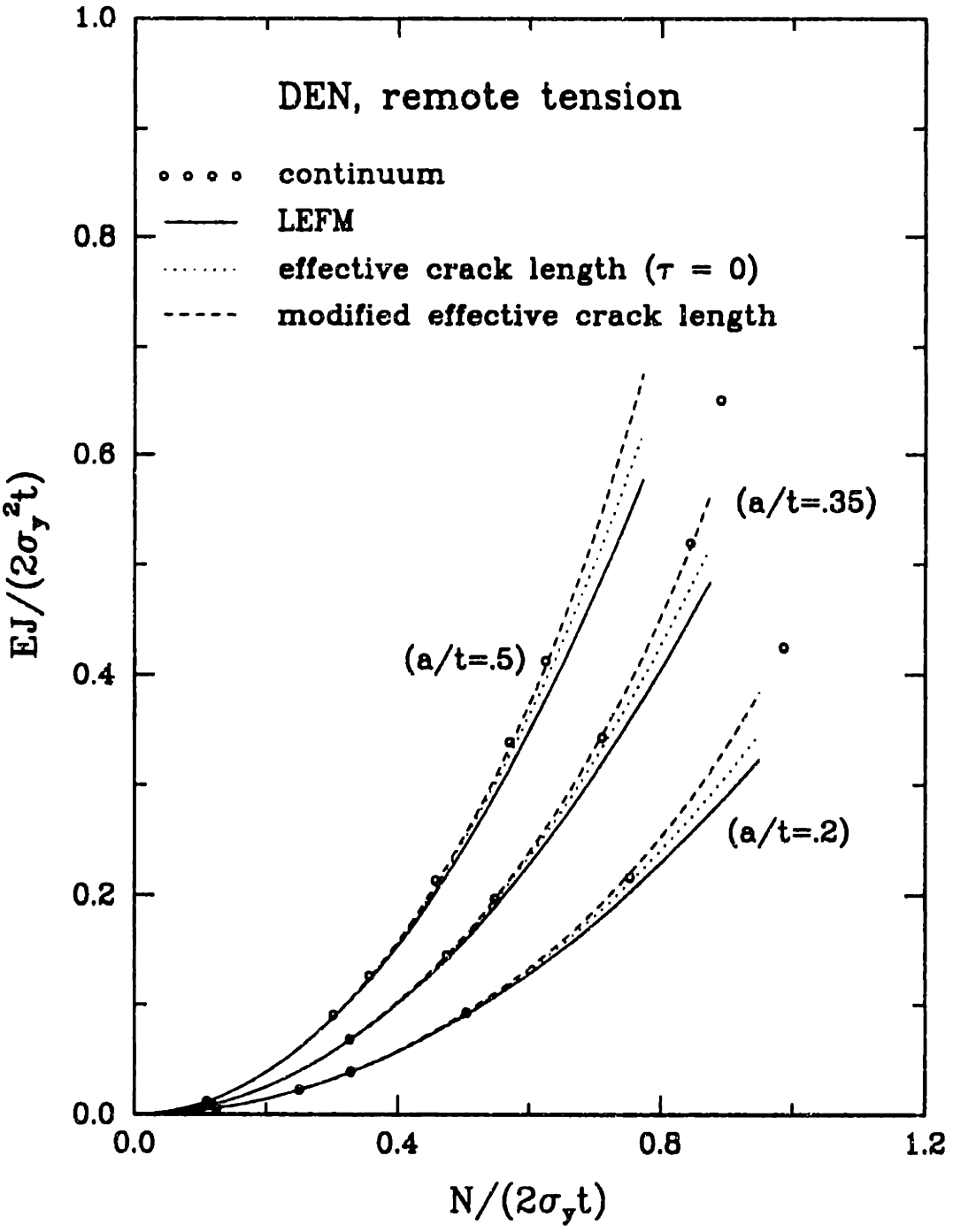


Figure 3.23: Normalized $J$ *vs.* axial force $N$ for remote tension of a plane strain *DEN*.

# Bibliography


[1] Anderson, T.L., 1991, *Fracture Mechanics, Fundamentals and Applications*, CRC Press, Inc., Boca Raton.

[2] Al-Ani, A. M., and Hancock, J. W., 1991, "*J*-Dominance of Short Cracks in Tension and Bending," *Journal of the Mechanics and Physics of Solids*, Vol. 39, No. 1, pp. 23-43.

[3] ASTM, 1983, Standard Test Method for Plane-Strain Fracture Toughness of Metallic Materials, *Annual Book of ASTM Standards*, E399-83, American Society for Testing and Materials, Philadelphia, PA.

[4] Barenblatt, G. I., 1962, "The Mathematical Theory of Equilibrium of Cracks in Brittle Fracture," *Advances in Applied Mechanics*, 7, pp. 55-129.

[5] Betegón, C., and Hancock, J. W., 1991, "Two-Parameter Characterization of Elastic-Plastic Crack-Tip Fields," *Journal of Applied Mechanics*, Vol. 58, pp. 104-110.

[6] Broek, D., 1982, *Elemantary Engineering Fracture Mechanics*, Martinus Nijhoff Publishers, The Hague.

[7] Du, Z.-Z., and Hancock, J. W., 1991, "The Effect of Non-Singular Stresses on Crack-Tip Constraint," *Journal of the Mechanics and Physics of Solids,* Vol. 39, pp. 555-567.

[8] Dugdale, D. S., 1960, "Yielding of Steel Sheets Containing Slits," *Journal of the Mechanics and Physics of Solids,* Vol. 8, pp. 100-108.

[9] Edmunds, T. M. and Willis, J. R., 1977, "Matched Asymptotic Expansions in Nonlinear Fracture Mechanics-III. In-Plane Loading of an Elastic Perfectly-Plastic Symmetric Specimen," *Journal of the Mechanics and Physics of Solids,* Vol. 25, pp. 423-455.

[10] Hibbitt, Karlsson and Sorensen, Inc., 1988, *ABAQUS User's Manual*, version 4.9, Hibbitt, Karlsson and Sorensen, Inc., Providence, RI.

[11] Hilton, P. D., Hutchinson, J. W., 1971, *Engineering Fracture Mechanics*, Vol. 3, pp. 435-451.

[12] Hutchinson, J. W., 1968, "Singular Behavior at the End of a Tensile Crack in a Hardening Material," *Journal of the Mechanics and Physics of Solids*, Vol. 16, pp. 13-31.

[13] Hutchinson, J. W., 1979, *A Course on Nonlinear Fracture Mechanics*, Dept. of Solid Mechanics, Technical University of Denmark, Lyngby.

[14] Irwin, G. R., 1958, "Fracture," in *Handbuch der Physik VI*, pp. 551-590, Flügge Ed., Springer, Berlin.

[15] Larsson, S. G., and Carlsson, A. J., 1973, "Influence of Non-singular Stress Terms and Specimen Geometry on Small-Scale Yielding at Crack Tips in Elastic-Plastic Material," *Journal of the Mechanics and Physics of Solids*, Vol. 21, pp. 263-277.

[16] Lee, H. and Parks, D. M., 1992, "Enhanced Elastic-Plastic Line-Spring Finite Element," submitted for publication.

[17] Leevers, P. S., and Radon, J. C., 1982, "Inherent Stress Biaxiality in Various Fracture Specimen Geometries," *International Journal of Fracture*, Vol. 19, pp. 311-325.

[18] McMeeking, R. M., 1977, "Finite Deformation Analysis of Crack-Tip Opening in Elastic-Plastic Materials and Implications for Fracture," *Journal of the Mechanics and Physics of Solids*, Vol. 25, pp. 357-381.

[19] McMeeking, R. M., and Parks, D. M., 1979, "On Criteria for $J$-Dominance of Crack-Tip Fields in Large-Scale Yielding," *Elastic-Plastic Fracture*, ASTM STP 668, American Society for Testing and Materials, Philadelphia, pp. 175-194.

[20] Parks, D. M., 1992 "Advances in Characterization of Elastic-Plastic Crack-Tip Fields," Chapter 2 in *Topics in Fracture and Fatigue*, Ed. A. S. Argon, Springer Verlag, New York.

[21] Press, W. H., et al., 1989, *Numerical Recipes, The Art of Scientific Computing*, Cambridge University Press, Cambridge.

[22] Rice, J. R., 1968, "A Path Independent Integral and the Approximate Analysis of Strain Concentrations by Notches and Cracks," *Journal of Applied Mechanics*, Vol. 35, pp. 379-386.

[23] Rice, J. R., 1972, "Some Remarks on Elastic Crack Tip Fields," *International Journal of Solids and Structures*, Vol. 8, pp. 751-758.

[24] Sham, T.–L., 1984, "A Finite-Element Study of the Asymptotic Near-Tip Fields for Mode I Plane-Strain Cracks Growing Stably in Elastic-Ideally Plastic Solids," *Elastic-Plastic Fracture: Second Symposium, Volume I - Inelastic Crack Analysis, ASTM STP 803*, C. F. Shih and J. P. Gudas, Eds., American Society for Testing and Materials, 1983, pp. I-52-I-79.

[25] Sham, T.–L., 1991, "The Determination of the Elastic $T$-term Using Higher Order Weight Functions," *International Journal of Fracture*, Vol. 48, pp. 81-102.

[26] Sham, T.–L., 1992, private communication.

[27] Tada, H., Paris, P. C., and Irwin, G. R., 1985, *The Stress Analysis of Cracks Handbook*, Fracture Proof Design, Saint Louis, MO.

[28] Tracey, D. M., 1976, "Finite Element Solutions for Crack-Tip Behavior in Small-Scale Yielding," *Journal of Engineering Materials and Technology*, Vol. 98, pp. 146-151.

[29] Van Dyke, M. D., 1968, *Perturbation Methods in Fluid Mechanics*, Academic Press, New York.

[30] Wang, Y.–Y., and Parks, D. M., 1990, "Evaluation of the Elastic $T$-stress in Surface-Cracked Plates Using Line-Spring Method," MIT report, August, 1990, to appear in *International Journal of Fracture*, 1992.

[31] Wang, Y.–Y., 1991, "A Two-Parameter Characterization of Elastic-Plastic Crack-Tip Fields and Applications to Cleavage Fracture," PhD. Thesis, Depart-

ment of Mechanical Engineering, Massachusetts Institute of Technology, Sept., 1991.

[32] Williams, M. L., 1957, "On the Stress Distribution at the Base of a Stationary Crack," *Journal of Applied Mechanics*, Vol. 24, pp. 111-114.

# Appendix

## Listing of the Program

```
C     ************************************************************
C     *                                                          *
C     *            Program Effective Cracklength                 *
C     *                                                          *
C     *  This program calculates the displacement q as a         *
C     *  function of load step Q. An effective crack-            *
C     *  length aeff is used to account for non-linearity        *
C     *  of the load/displacement curve due to crack-tip         *
C     *  plasticity in the transition from the linear            *
C     *  elastic to the fully plastic regime.                    *
C     *                                                          *
C     *                by Dagmar E. Hauf                         *
C     *                                                          *
C     ************************************************************

      program effective cracklength
      implicit real*8(a-h, o-z)
      external fkhat, sqkhat, dkhat
      open(unit=19, file='inp.dat', status='unknown')
      open(unit=20, file='res.dat', status='unknown')
      open(unit=21, file='res1.dat', status='unknown')
      open(unit=22, file='res2.dat', status='unknown')
      read (19,*) epsil, numits, ainit, Qlimit, sigy, t,
     & Cinit, H, poiss, E, mark
      z = 0.d+00
      aeff = ainit
      dq = Qlimit / (numits-1)
      do 10 i=1, numits
         Q = (i-1) * dQ
         call newt(aeff, ainit, epsil, Q, sigy, t, mark)
         call qgaus (sqkhat, z, aeff, sta, t)
         C = Cinit + (2 / H) * sta
         Cinv = 1/C
         qsmall = C * Q
```

```
         fkone = fkhat(aeff, t) * Q/t
         eprime = E / (1 - (poiss ** 2))
         fjint = (fkone ** 2) / eprime
         write (20,15) qsmall, Q
         write (21,15) Q, aeff
         write (22,15) Q, fjint
   10 continue
   15 format(1(PE15.7),4x,1(PE15.7))
      stop
      end

C     ********************************************************
C     *  Newton-Raphson                                      *
C     *  This subroutine returns to the main program the     *
C     *  effective cracklength aeff corresponding to the     *
C     *  load step Q                                         *
C     ********************************************************
      subroutine newt(aeff, ainit, epsil, Q, sigy, t, mark)
      implicit real*8(a-h, o-z)
      open (unit=30, file='daeff.dat', status='unknown')
      if (mark.eq.1) then
         go to 1
      else
         go to 2
      endif
    1 Do 11 n=1, 20
         call funcd(aeff, ainit, Q, f, df, sigy, t)
         daeff = f/df
         aeff = aeff - daeff
         write (30, *) Q, aeff, dabs(daeff), epsil
         if(dabs(daeff).lt.epsil) return
   11 continue
    2 Do 12 n=1, 20
         call funcdt(aeff, ainit, Q, f, df, sigy, t)
         daeff = f/df
         aeff = aeff - daeff
         write (30, *) Q, aeff, dabs(daeff), epsil
         if(dabs(daeff).lt.epsil) return
   12 continue
      pause 'aeff exceeding maximum iterations'
      end

C     ********************************************************
C     *  This subroutine defines the equations f and df      *
C     *  (derivative of f wrt the effective cracklength)     *
C     *  to be solved with Newton-Raphson                    *
C     ********************************************************
      subroutine funcd(aeff, ainit, Q, f, df, sigy, t)
      implicit real*8(a-h, o-z)
      eins = 0.019 * (Q / (sigy * t)) ** 2
      f = aeff - ainit - (eins * fkhat(aeff, t) ** 2)
      df = 1  - (eins * 2 * fkhat(aeff, t) * dkhat(aeff, t))
      return
      end
```

```
      subroutine funcdt(aeff, ainit, Q, f, df, sigy, t)
      implicit real*8(a-h, o-z)
      open (unit=29, file='plast.dat', status='unknown')
      call flam(aeff, Q, sigy, t, rflam, drflam)
      eins = (Q / (sigy * t)) ** 2
      plast = eins * rflam * fkhat(aeff, t) ** 2
      f = aeff - ainit - plast
      df = 1  - eins * (drflam * fkhat(aeff, t) ** 2 +
     & rflam * 2 * fkhat(aeff, t) * dkhat(aeff, t))
      plcon = 16 * plast
      geocon = t - aeff
      write (29, *) Q, plcon, aeff, geocon
      return
      end

C     ************************************************************
C     *  Gaussian Integration                                    *
C     *  This subroutine integrates the geometric function       *
C     *  sqkhat from zero to the effective cracklength for       *
C     *  further calculation of the compliance C in the          *
C     *  main program                                            *
C     ************************************************************
      subroutine qgaus(func, a, b, ss, t)
      implicit real*8(a-h, o-z)
      dimension x(5), w(5)
      data x/.1488743389d+00,.4333953941d+00,.6794095682d+00,
     & .8650633666d+00,.9739065285d+00/
      data w/.2955242247d+00,.2692667193d+00,.2190863625d+00,
     & .1494513491d+00,.0666713443d+00/
      xm = 0.5d+00 * (b + a)
      xr = 0.5d+00 * (b - a)
      ss = 0
      do 11 j=1,5
         dx=xr*x(j)
         ss=ss+w(j)*(func(xm+dx, t) + func(xm - dx, t))
   11 continue
      ss=xr * ss
      return
      end

C     ************************************************************
C     *  Geometric function fkhat for a single edge notch        *
C     *  test specimen from Tada et al.                          *
C     ************************************************************
      function fkhat(aeff, t)
      implicit real*8(a-h, o-z)
C     open (unit =23, file='khat.dat', status='unknown')
      pi = 3.141592654d+00
      x = (pi * aeff) / (2.0 * t)
      aot = aeff / t
      sin3 = (1 - dsin(x)) ** 3
      arg =  2.0 * t * dtan(x)
      f1 = dsqrt(arg)
      f2b = 0.752 + (2.02 * aot) + (0.37 * sin3)
```

```
      f2 = f2b / dcos(x)
      fkhat = f1 * f2
C     write (23,*) fkhat
      return
      end

C     ********************************************************
C     *  Square of the geometric function fkhat used         *
C     *  in the Gaussian Integration                         *
C     ********************************************************
      function sqkhat(aeff, t)
      implicit real*8(a-h, o-z)
C     open (unit=24, file='sqkhat.dat', status='unknown')
      pi = 3.141592654d+00
      x = (pi * aeff) / (2.0 * t)
      aot = aeff / t
      sin3 = (1 - dsin(x)) ** 3
      arg =  2.0 * t * dtan(x)
      f1 = dsqrt(arg)
      f2b = 0.752 + (2.02 * aot) + (0.37 * sin3)
      f2 = f2b / dcos(x)
      sqkhat = (f1 * f2) ** 2
C     write (24, *) sqkhat
      return
      end

C     ********************************************************
C     *  Derivative of the geometric function fkhat          *
C     *  wrt the effective cracklength aeff                  *
C     ********************************************************
      function dkhat(aeff, t)
      implicit real*8(a-h, o-z)
C     open (unit=25, file='dkhat.dat', status='unknown')
      pi = 3.141592654d+00
      x = (pi * aeff) / (2.0 * t)
      aot = aeff / t
      pif = pi / (2.0 * t)
      sin2 = (1 - dsin(x)) ** 2
      sin3 = (1 - dsin(x)) ** 3
      tan2 = 1 + (dtan(x)) ** 2
      arg =  dtan(x)
      f1 = dsqrt(arg)
      f2b = 0.752 + (2.02 * aot) + (0.37 * sin3)
      f2 = f2b / dcos(x)
      df1 = 0.5 * (1 / f1 ) * pif * tan2
      df2b = (2.02 / t) - (1.11 * pif * dcos(x) * sin2)
      df2 = (df2b + (f2b * pif * dtan(x))) / dcos(x)
      dkhat = ((df1 * f2) + (f1 * df2)) * dsqrt(2.0 * t)
C     write (25, *) dkhat
      return
      end
```

```
C     ********************************************************
C     *  Interpolating polynomial for the ratio of           *
C     *  plastic zone size to the plastic zone size          *
C     *  at zero T-stress                                    *
C     ********************************************************
      subroutine flam(aeff, Q, sigy, t, rflam, drflam)
      implicit real*8(a-h, o-z)
      open (unit=26, file='flam.dat', status='unknown')
      c0 = -0.001d+00
      c1 = -0.539d+00
      c2 = 0.375d+00
      c3 = 0.236d+00
      c4 = 0.974d+00
      fnat = 2.302585093d+00
      beta = 0.12
      tau = (that(aeff, t) * Q) / (sigy * t)
      dtau = (dthat(aeff, t) * Q) / (sigy * t)
      taupo = c0 + (c1 * tau) + (c2 * tau ** 2) + (c3 * tau ** 3) +
     & (c4 * tau ** 4)
      dtaupo = (c1 * dtau) + (2 * c2 * tau * dtau) +
     & (3 * c3 * (tau ** 2) * dtau) + (4 * c4 * (tau ** 3) * dtau)
      rflam = beta * 0.15 * (10 ** taupo)
      drflam = beta * 0.15 * dtaupo * fnat * (10 ** taupo)
      write (26, *) rflam, drflam
      return
      end

C     ********************************************************
C     *  T-stress calibration function for a SEN specimen    *
C     ********************************************************
      function that(aeff, t)
      implicit real*8(a-h, o-z)
      open (unit=27, file='that.dat', status='unknown')
      a0 = -0.211d+00
      a1 = -5.86d+00
      a2 = 31.8d+00
      a3 = -74.9d+00
      a4 = 65.6d+00
      aot = aeff / t
      that = a0 + (a1 * aot) + (a2 * (aot ** 2)) + (a3 *(aot ** 3)) +
     & (a4 * (aot **4))
      write (27, *) that
      return
      end

C     ********************************************************
C     * Derivative of T-stress calibration function for      *
C     * a SEN specimen                                       *
C     ********************************************************
      function dthat(aeff, t)
      implicit real*8(a-h, o-z)
      open (unit=28, file='dthat.dat', status='unknown')
```

```
      a1 = -5.86d+00
      a2 = 31.8d+00
      a3 = -74.9d+00
      a4 = 65.6d+00
      aot = aeff / t
      oot = 1 / t
      dthat = (a1 * oot) + (2 * a2 * aot * oot) +
     & (3 * a3 * (aot ** 2) * oot) + (4 * a4 * (aot ** 3) * oot)
      write (28, *) dthat
      return
      end
```